Monthly Notices
of the
ROYAL ASTRONOMICAL SOCIETY

MNRAS **454,** 2890–2908 (2015) doi:10.1093/mnras/stv2106

Non-singular orbital elements for special perturbations in the two-body problem

Giulio Baù,[1]★ Claudio Bombardelli,[2] Jesús Peláez[2] and Enrico Lorenzini[3]

[1]*Department of Mathematics, University of Pisa, Largo Pontecorvo 5, I-56127 Pisa, Italy*
[2]*Department of Applied Physics, Technical University of Madrid, Plaza Cardenal Cisneros 3, E-28040 Madrid, Spain*
[3]*Department of Industrial Engineering, University of Padova, Via Venezia 1, I-35131 Padova, Italy*

Accepted 2015 September 8. Received 2015 September 5; in original form 2015 July 29

ABSTRACT

Seven spatial elements and a time element are proposed as the state variables of a new special perturbation method for the two-body problem. The new elements hold for zero eccentricity and inclination and for negative values of the total energy. They are developed by combining a spatial transformation into projective coordinates (as in the Burdet–Ferrándiz regularization) with a time transformation in which the exponent of the orbital radius is equal to one instead of two (as commonly done in the literature). By following this approach, we discover a new linearization of the two-body problem, from which the orbital elements can be generated by the variation of parameters method. The geometrical significance of the spatial quantities is revealed by a new intermediate frame which differs from a local vertical local horizontal frame by one rotation in the instantaneous orbital plane. Four elements parametrize the attitude in space of this frame, which in turn defines the orientation of the orbital plane and fixes the departure direction for the longitude of the propagated body. The remaining three elements determine the motion along the radial unit vector and the orbital longitude. The performance of the method, tested using a series of benchmark orbit propagation scenarios, is extremely good when compared to several regularized formulations, some of which have been modified and improved here for the first time.

Key words: methods: numerical – celestial mechanics – minor planets, asteroids: general.

1 INTRODUCTION

With the rapid development of punched-card machines in the late 1930s, computation of orbits of celestial bodies by automatic methods became a common practice. Paul Herget, the first director of the Minor Planets Center (MPC), was a pioneer in the use of machine methods for minor planets ephemeris computation. In 1947, he started to adopt the special perturbations approach to predict planetary motions (Marsden 1980). Due to the limited computational capacity available at that time, special perturbation schemes based on the variation of parameters (VOP) became an attractive alternative to Cowell's and Encke's formulations mainly because in many problems the same accuracy could be achieved with a larger integration step (Herrick 1948). Among the different VOP approaches, the classical elliptic elements were not well suited to the purpose, since more simple, symmetrical equations and more uniform operations were desirable (Musen 1954). On the other hand, it was known that special perturbations of orbital elements based on vectorial integrals of the two-body problem (vectorial elements) enjoy all these properties.

Strömgren's VOP method (Strömgren 1929; Musen 1954) was the first to be derived by means of vector calculus, and the MPC implemented it to calculate first-order perturbations of planets (Marsden 1980). However, the breakthrough in the use of vectorial elements came from Milanković (1939), who derived the equations of the eccentricity and angular momentum vectors ($\boldsymbol{e}$ and $\boldsymbol{h}$) in Lagrangian form for general planetary perturbations. Following the same idea, Herrick (1948, 1953) replaced five of the classical elliptic elements by the vectors $\boldsymbol{e}$, $\boldsymbol{h} \times \boldsymbol{e}$, and integrated the corresponding differential equations to determine the special perturbations of the asteroid Icarus. His formulation was superior to Strömgren's for ephemeris computation, because the directions of the major and minor axes of the osculating ellipse ($\boldsymbol{a}$ and $\boldsymbol{b}$) are obtained in a much more direct and fast way. Musen (1954) improved Herrick's method by choosing $\boldsymbol{h} \times \boldsymbol{e}/p$ (where p is the semilatus rectum) and $\boldsymbol{h}$ as elements, and the algorithm was extensively applied to the minor bodies of the Solar system (Herget 1962; Marsden 1980). The vectorial method was exploited by Musen (1960, 1961b) to study also the perturbed motion of an artificial satellite around the Earth.

An exhaustive survey of vectorial orbital elements of the Milanković type for both special and general perturbations of the two-body problem is found in Rosengren & Scheeres (2014). All these methods do not present the singularity for zero inclination

★ E-mail: bagiugio@gmail.com

because the classical Euler angles (Ω, i, ω for the longitude of the node, inclination, argument of pericentre, respectively) are replaced by the direction cosines of the perifocal basis $\{\boldsymbol{a}, \boldsymbol{b}, \boldsymbol{k}\}$, with $\boldsymbol{k} = \boldsymbol{a} \times \boldsymbol{b}$ perpendicular to the orbital plane. However, the unit vectors $\boldsymbol{a}$ and $\boldsymbol{b}$ become meaningless when the eccentricity is zero.[1] This intrinsic singularity produces small divisors in the differential equations, which bring to a deleterious loss of accuracy in the numerical integration of near circular motion (Herget 1962). The difficulty can be avoided in the vectorial elements with a simple change of variables (for example, by employing $\boldsymbol{e}$ and $\boldsymbol{h} \times \boldsymbol{e}$ instead of $\boldsymbol{a}$ and $\boldsymbol{b}$), while it is impossible to eliminate from the equation that governs the angular displacement of the propagated object with respect to $\boldsymbol{a}$ (Musen 1954). Indeed, one way to remove also this singularity is to reckon the angular position from a *departure point* (here denoted by $\boldsymbol{s}$) which lies on the orbital plane, is fixed along a Keplerian motion, and does not depend on the orientation of the apsidal line. One of the first sets of non-singular elements (i.e. valid for zero inclination and zero eccentricity) for special perturbations is due to Pines (1961). The departure direction is given by the initial position on the osculating orbit, which, along with the initial velocity, are the parameters chosen to describe the motion. Pines' elements are canonical (Cohen & Hubbard 1962) and avoid the additional equation for the variable related to the angular displacement along the osculating ellipse.

The concept of a departure point, introduced by Hansen (1857, p. 71), suggests that a possible way to obtain non-singular elements (not necessarily vectorial) is to refer the motion to an *intermediate frame* $\{\mathrm{F}; \boldsymbol{s}, \boldsymbol{t}, \boldsymbol{k}\}$, with the origin F at one focus of the osculating conic and where $\boldsymbol{t} = \boldsymbol{k} \times \boldsymbol{s}$. In the well-known set of equinoctial elements investigated by Broucke & Cefola (1972) and in all its variations (Hintz 2008), the orbital position is recovered from the departure point by means of the true longitude $L = \varpi + f$, where $\varpi = \Omega + \omega$ and f is the osculating true anomaly. It follows that the orientation of the equinoctial frame depends only on Ω and i. The timing along the orbit is controlled by the mean longitude at the epoch which is free of singularities. The computation of L requires to solve Kepler's equation written in terms of the eccentric longitude, unless this is chosen as the independent variable in place of the physical time (Fukushima 2008). Herrick (1953) modified his original method by replacing the mean anomaly with the mean longitude in the equinoctial frame. The equinoctial true and mean longitudes have been recently adopted by Rosengren & Scheeres (2014) in substitution of the time of pericentre passage for deriving non-singular equations of Milanković's vectorial elements, both in Lagrangian and Gaussian form.

The *ideal* coordinates were conceived by Hansen (1857, p. 66) to develop a theory of general perturbations of minor planets (see also Brown 1896, chapter X). The reference frame $\{\mathrm{F}; \boldsymbol{s}, \boldsymbol{t}, \boldsymbol{k}\}$, where $\boldsymbol{s}$ is placed at a departure point, is ideal if the component along $\boldsymbol{k}$ of its angular velocity is zero (Deprit 1976). The condition that $\boldsymbol{s}$ is fixed in the plane of the orbit reflects on the constraint $\mathrm{d}\sigma + \cos i \, \mathrm{d}\Omega = 0$, where the pseudo-element σ is the angle measured positively eastwards from the ascending node to $\boldsymbol{s}$.[2] The longitude of the propagated object is an ideal coordinate and is given by $\phi = \chi + f$, where $\chi = \omega - \sigma$ (Brown 1896, p. 163). An attractive property of the ideal frames is that the equation of motion projected along the axes of $\boldsymbol{s}$ and $\boldsymbol{t}$ (Hansen 1857, p. 69; Broucke, Lass & Ananda 1971, equation 53) take the same form as in a fixed frame. A separation is therefore achieved to some extent between the motion in the orbital plane and the rotation of the ideal frame. Garofalo (1960) chose as elements the direction cosines of the ideal axes with respect to fixed rectangular axes, the angular momentum h, and the projections of the vector $\boldsymbol{e}/p$ along $\boldsymbol{s}$ and $\boldsymbol{t}$. The true longitude ϕ is also included in this set. A similar, but much less-redundant system of equations was obtained by Herget (who seems unaware of Garofalo's work) by using Rodrigues' parametrization of a finite rotation (Rodrigues 1840, p. 400) in the form given by Cayley (1843, i.e. Gibbs' rotation vector). Instead of ϕ, the author picks as angular variable the sum of the perturbed portion of the mean anomaly and the pseudo-element χ (as Strömgren already did; see Musen 1954, equation 32).

Cayley's vector works also when the inclination is zero, but it fails for half turns. On the other hand, Euler parameters (Whittaker 1917, p. 8) allow us to remove any singularity with the addition of just one redundant variable. They were introduced by Broucke et al. (1971), Vitins (1978), Chelnokov (1992), Sharaf, Awad & Najmuldeen (1992), and Peláez, Hedo & de Andrés (2007) in relation to the local vertical local horizontal frame (hereafter it will be called orbital frame), and by Musen (1964), Hestenes (1983, where they form a spinor), and Gurfil (2005) for the perifocal frame. The non-singular set of elements developed by Cohen & Hubbard (1962) includes a quaternion that brings information about the angular momentum and the attitude of an intermediate frame. As concerns the ideal coordinate system, the Euler parameters are employed by Musen (1958) in a special perturbation method based on Hansen's theory. Deprit (1975) suggested their use to improve Herget's formulation. After explaining the geometrical significance of Hansen's ideal frame, the motion in the orbital plane is described by the ideal mean longitude (denoted by U in Herget 1962, equation 51), and three elements almost identical to those presented by Herget and Garofalo.

So far we have seen that the definition of a suitable intermediate frame is a powerful tool for generating non-singular elements. A different approach consists in regularizing the two-body problem (see for example the introduction in Baù, Bombardelli & Peláez 2013), so that the solution of the transformed linear system can be written explicitly. The resulting constants of integration are regarded as new variables to describe the perturbed motion. Stiefel & Scheifele (1971, section 19) and Burdet (1968, 1969) derived from the Kustaanheimo–Stiefel (K–S; Kustaanheimo & Stiefel 1965; Stiefel & Scheifele 1971, chapter 2) and Sperling's regularizations (Sperling 1961; Burdet 1967), respectively, non-singular elements for vanishing eccentricity, inclination, and orbital radius. Chelnokov (1992) showed that the K–S variables can be related to a unit quaternion. Its components represent a coordinate system which has one axis oriented along the radial direction $\boldsymbol{i}$ and does not rotate around $\boldsymbol{i}$ at any time. In the absence of perturbations, the unit quaternion is the solution of an harmonic oscillator of frequency one half with respect to the true anomaly. Then (Chelnokov 1993), two quaternions are introduced by the VOP method as part of a set of non-singular elements.

In Burdet's focal method (Burdet 1969) the position vector is decomposed into the product of the orbital radius (r) and the radial unit vector, which after Ferrándiz (1988) are called *projective coordinates*. The reciprocal radius ρ and the vector $\boldsymbol{i}$ satisfy linear differential equations in the pure two-body motion if the transformation $\mathrm{d}t = r^2 \, \mathrm{d}s$, from the time t to the independent variable s,

[1] Strömgren's method and its modified version proposed by Musen (1961a) to compute higher order effects, employ as vectorial quantities the angular velocity vector and Gibbs' vector semitangent of version (Wilson 1901, p. 340) of the perifocal frame, respectively.

[2] The definition of pseudo-element is given in Brown (1896, p. 74). Note that the author adopts the opposite convention for the angle σ.

is applied. The constants that were attached to ρ, $\boldsymbol{i}$, and t, along with the semilatus rectum, are topologically regular elements, but are not defined at collision (Stiefel & Scheifele 1971, p. 78). As we learn from Flury & Janin (1975), Burdet derived an analogous set of focal elements by taking as independent variable the true longitude ϕ instead of s. With this choice, the oscillation frequency of the variables ρ, $\boldsymbol{i}$ is equal to one for Keplerian motions and so their evolution become Lyapunov stable (Vitins 1978; Fukushima 2007a, appendix C2). Moreover, Vitins (1978), first noted that the normal form of the differential equation for the radial unit vector naturally leads to introduce the orbital frame. Then, he suggested to use Euler parameters to represent this frame, thus eliminating two redundant variables from Burdet's original formulation, and still preserving the stability of the corresponding system.

The VOP scheme of Peláez et al. (2007), referred to as Dromo, was derived from the same equations of the improved Burdet's method reported in Vitins (1978). In Dromo, the variables of integration are: the physical time, four Euler parameters associated with an ideal frame named departure frame,[3] the inverse angular momentum (q_3), and the projections of the vector $q_3\,\boldsymbol{e}$ on two orthogonal axes of a second ideal frame which, in general, does not coincide with the departure frame.[4] Even if Dromo and Deprit's formulations implement almost the same spatial elements, the former is more advantageous for numerical integration. In fact, the analytic step-size control (Stiefel & Scheifele 1971, p. 77) induced by the fictitious time ϕ greatly improves the performance achievable with a fixed step-size integrator. Besides, the time element included by Deprit in order to recover ϕ works only for elliptic motion. On the other hand, in Dromo such angle is directly provided by the independent variable itself, which is well defined for any non-degenerate conic. A consequent benefit is that Kepler's equation does not need to be solved.

The independent variable ϕ of Dromo is related to the time t by $\mathrm{d}t = r^2 q_3\,\mathrm{d}\phi$. In Baù et al. (2013), a modified form of this time transformation, borrowed from Sharaf et al. (1992), was adopted to derive generalized Dromo elements which are more advantageous for conservative forces. The key step is to define a generalized angular momentum by including the disturbing potential in the contribution of the kinetic energy due to the transverse component of the velocity. Time elements for the generalized counterparts of Dromo elements were developed in Baù & Bombardelli (2014) to reduce the integration error in the physical time. We have recently discovered that a similar set of elements as in Baù et al. (2013) with one of the time elements in Baù & Bombardelli (2014) was derived by Vitins (1978).

Numerical tests to evaluate the performance of non-singular elements for orbit computation appeared in the early 1970s. While Stiefel & Scheifele (1971, section 23) and Bond (1974) report the results of their own elements only, Burdet (1968) includes Encke's method and a set of K–S elements taken from Stiefel et al. (1967), in addition to his natural elements. Comparisons with Cowell's method were undertaken by Dallas & Rinderle (1974), Velez et al. (1974), Flury & Janin (1975), and revealed that VOP methods are increasingly more accurate for the same computational cost as the perturbations become weaker and more complicated to calculate. In later years, the use of VOP schemes for special perturbations fell into oblivion, out of which it was recalled by Ferrándiz, Sansaturio & Vigo (1991), Palacios & Calvo (1996), Arakida & Fukushima (2001), and Barrio & Serrano (2008). More recently, Baù et al. (2013) and Baù & Bombardelli (2014) investigated the behaviour of the generalized Dromo elements with and without a time element for perturbed motion around the Earth. It turns out that these formulations substantially improve the original method of Peláez et al. (2007), and show an excellent performance when propagating circular to moderately eccentric perturbed orbits. However, at high eccentricities the benefit of the spatial elements is partly obscured by the lower performance of the time (or time element) integration compared to methods constructed on a time transformation of the Sundman type (i.e. linear in the orbital radius). This is especially true with third-body perturbations and when employing fixed step-size integrators.

These facts motivate the effort to develop in the framework of the projective decomposition a new set of elements starting from a classical Sundman transformation of the physical time. Such task is the focus of the paper. Since the method is proposed as a companion procedure to be used when the enhanced versions of Dromo become less efficient, our test campaigns deal with perturbed orbits of high eccentricity. More specifically, we consider two examples representative of weak and moderate perturbations, and a third case with a more realistic propagation around the Earth. The performance of the new non-singular elements is assessed with respect to several other sets of regular elements, regularizations, and a stabilized form of Cowell's method.

The paper is organized as follows. Section 2 gives a brief description of the new method. In Section 3, we address the radial motion and introduce the first three elements. Section 4 is devoted to the time element. In Section 5, we define the intermediate frame and the related Euler parameters, first in a geometrical way, and then by following a VOP approach. Section 6 collects the differential equations of the elements and illustrates the implementation for carrying out a numerical integration with our method. Section 7 contains the results on the performance, and Section 8 reports the conclusions. Finally, in the appendices we derive non-obvious relations given in the theory and we describe the modifications that we have applied to improve some formulations selected for the numerical tests.

2 OVERVIEW OF THE NEW FORMULATION

In the same way as in Stiefel & Scheifele (1971, p. 87) we change the independent variable through a Sundman transformation of the physical time into the angle φ. In the case of unperturbed motion, the quantity φ coincides, up to an additive constant, to the eccentric anomaly. Complying with the approach of the projective decomposition, which is the starting step towards Burdet's regularization, we deal with the displacement along the radial direction. In the two-body problem, the second-order differential equation of the orbital radius can be linearized. Its solution contains two integration constants (λ_1, λ_2) that are seen as the projections of a generalized eccentricity vector on two orthogonal axes. This geometrical interpretation leads to define an intermediate frame and thereby a departure point on the osculating plane. The quantities λ_1, λ_2, the total energy λ_3, and the fictitious time φ determine the orbital radius and the angle between the radial unit vector and the departure point. In order to obtain the position, we just need to know the attitude of the intermediate frame, and to this end, Euler parameters (denoted

[3] If at the initial epoch the departure point of the ideal coordinate system introduced by Deprit (1975) is located by the position vector, then at any epoch the departure frame coincides with Deprit's ideal frame up to a rotation of 90° around the radial direction. This discrepancy is due to the definition of the orbital frame given in Peláez et al. (2007, equation 2).

[4] The two frames differ by a rotation around the common axis normal to the orbital plane equal to the initial value of the independent variable.

by λ_4, λ_5, λ_6, λ_7) are employed. We show that these four elements can be generated also from a VOP approach: the idea is to identify a reference frame such that its angular velocity along a pure two-body motion is constant with respect to the independent variable φ. Then, Euler parameters associated with this frame obey linear first-order differential equations, and their solution can be expressed in terms of our four elements. To our knowledge, linearized equations of Euler parameters have never been published before for a time transformation in which the orbital radius has exponent one.

The motion in the variable φ is completely described by the elements λ_i, $i = 1 \ldots 7$, and the physical time is determined from Kepler's equation by a time element. This set is non-singular at zero inclination and eccentricity, works for negative values of the total energy, and is undefined for collision orbits. A peculiar aspect of the formulation is that the disturbing potential is required to calculate the velocity, and, in particular, it must be independent on the osculating angular momentum.

3 MOTION IN THE ORBITAL PLANE

Let us consider a body of mass m (the propagated object) and denote with $\boldsymbol{r}$ and $\boldsymbol{v}$ its position and velocity relative to an other body of mass M (the primary). In a reference frame with the origin F at the primary's centre of mass and with fixed axes, the equation of motion of the propagated object is

$$\frac{\mathrm{d}^2\boldsymbol{r}}{\mathrm{d}t^2} = -\frac{k^2\,(m+M)}{r^3}\boldsymbol{r} + \boldsymbol{F}, \tag{3.1}$$

where k^2 is the gravitational constant, $r = |\boldsymbol{r}|$ is the orbital radius, and t is the time variable. The first term on the right-hand side represents the gravitational attraction exerted by the primary and $\boldsymbol{F}\,(t, \boldsymbol{r}, \boldsymbol{v})$ is usually referred to as the perturbing force. The latter can be expressed as

$$\boldsymbol{F} = -\frac{\partial\,\mathcal{U}}{\partial\,\boldsymbol{r}} + \boldsymbol{P}, \tag{3.2}$$

where $\mathcal{U}\,(t, \boldsymbol{r})$ is the disturbing potential energy per unit mass and $\boldsymbol{P}\,(t, \boldsymbol{r}, \boldsymbol{v})$ includes the perturbations that do not arise from a disturbing potential.

Let the vector $\boldsymbol{h} = \boldsymbol{r} \times \boldsymbol{v}$ be the angular momentum per unit mass and $h = |\boldsymbol{h}|$. We introduce the orbital frame $\mathcal{O} = \{\mathrm{F}; \boldsymbol{i}, \boldsymbol{j}, \boldsymbol{k}\}$, with

$$\boldsymbol{k} = \frac{\boldsymbol{h}}{h}, \quad \boldsymbol{i} = \frac{\boldsymbol{r}}{r}, \quad \boldsymbol{j} = \boldsymbol{k} \times \boldsymbol{i}. \tag{3.3}$$

In this orthonormal basis the velocity takes the form

$$\boldsymbol{v} = \frac{\mathrm{d}r}{\mathrm{d}t}\,\boldsymbol{i} + \frac{h}{r}\,\boldsymbol{j}, \tag{3.4}$$

and the components of the perturbing force are denoted by

$$R = \boldsymbol{F}\cdot\boldsymbol{i}, \quad T = \boldsymbol{F}\cdot\boldsymbol{j}, \quad N = \boldsymbol{F}\cdot\boldsymbol{k}. \tag{3.5}$$

For later use, we report below the angular velocity of the orbital frame (Deprit 1975, equation 14):

$$\boldsymbol{w}_{\mathcal{O}} = N\,\frac{r}{h}\,\boldsymbol{i} + \frac{h}{r^2}\,\boldsymbol{k}. \tag{3.6}$$

From here on, we shall adopt dimensionless quantities: the units of length and time are chosen in such a way that the constant $k^2(m + M)$ is replaced by 1, and m is taken as the unit of mass. The proposed approach follows the idea inherited from Burdet's linearization of considering the motion as the composition of the radial displacement r along the unit vector $\boldsymbol{i}$ with the rotation of $\boldsymbol{i}$ in space (r, $\boldsymbol{i}$ are named projective coordinates after Ferrándiz 1988).

3.1 Radial motion

Let us compute the time derivative of $\boldsymbol{v}$ (equation 3.4) taking advantage of (3.6), and plug the resulting expression into the left-hand side of equation (3.1). After projecting this equation along the radial direction $\boldsymbol{i}$ and considering (3.5), we find that (Baù et al. 2013, equation 9)

$$\frac{\mathrm{d}^2r}{\mathrm{d}t^2} = \frac{h^2}{r^3} - \frac{1}{r^2} + R. \tag{3.7}$$

In order to apply the VOP technique in an exact way we try to transform (3.7) into a linear differential equation. To this end, we first introduce a new independent variable, the fictitious time φ, by means of the time transformation

$$\frac{\mathrm{d}t}{\mathrm{d}\varphi} = \frac{r}{\sqrt{-2\,\varepsilon}}, \tag{3.8}$$

where ε is the total energy which is expressed with the aid of (3.4) as

$$2\,\varepsilon = \left(\frac{\mathrm{d}r}{\mathrm{d}t}\right)^2 + \left(\frac{h}{r}\right)^2 - \frac{2}{r} + 2\mathcal{U}. \tag{3.9}$$

From here on, we make the hypothesis that the total energy is strictly negative ($\varepsilon < 0$). In the case of Keplerian motion the quantity φ represents, up to an additive constant, the eccentric anomaly. The radial velocity and acceleration can be written as

$$\frac{\mathrm{d}r}{\mathrm{d}t} = \frac{\sqrt{-2\,\varepsilon}}{r}\,\frac{\mathrm{d}r}{\mathrm{d}\varphi}, \tag{3.10}$$

$$\frac{\mathrm{d}^2r}{\mathrm{d}t^2} = \frac{-2\,\varepsilon}{r^2}\left[\frac{\mathrm{d}^2r}{\mathrm{d}\varphi^2} - \frac{1}{r}\left(\frac{\mathrm{d}r}{\mathrm{d}\varphi}\right)^2\right] - \frac{1}{r^2}\,\frac{\mathrm{d}r}{\mathrm{d}\varphi}\,\frac{\mathrm{d}\varepsilon}{\mathrm{d}\varphi}. \tag{3.11}$$

Next, the expression given in (3.10) is inserted in (3.9) and, by rearranging the terms, we derive the useful relation

$$\left(\frac{\mathrm{d}r}{\mathrm{d}\varphi}\right)^2 = \frac{h^2 + 2\,r^2\,\mathcal{U}}{2\,\varepsilon} - r^2 - \frac{r}{\varepsilon}. \tag{3.12}$$

Equations (3.11) and (3.12) are employed to transform (3.7) into

$$\frac{\mathrm{d}^2r}{\mathrm{d}\varphi^2} + r - \lambda_3 = (R\,r - 2\mathcal{U})\,\lambda_3\,r + \frac{1}{2\lambda_3}\,\frac{\mathrm{d}\lambda_3}{\mathrm{d}\varphi}\,\frac{\mathrm{d}r}{\mathrm{d}\varphi}, \tag{3.13}$$

where we have introduced the generalized semimajor axis

$$\lambda_3 = -\frac{1}{2\,\varepsilon}. \tag{3.14}$$

The relation above is differentiated by use of (3.8) and of the well-known formula for the time derivative of the total energy (see for instance Stiefel & Scheifele 1971, p. 11, equation 16, wherein h is replaced by $-\varepsilon$) to get

$$\frac{\mathrm{d}\lambda_3}{\mathrm{d}\varphi} = 2\,\lambda_3^{5/2}\,r\left(\boldsymbol{P}\cdot\boldsymbol{v} + \frac{\partial\,\mathcal{U}}{\partial\,t}\right), \tag{3.15}$$

with $\partial/\partial\,t$ denoting the partial derivative with respect to the physical time. Therefore, it is evident that the right-hand side of equation (3.13) vanishes when perturbations are not present ($\mathcal{U}$ and $\boldsymbol{P}$ are both equal to zero).

We conclude that by introducing the fictitious time φ through the time transformation (3.8) and embedding the total energy integral in the form provided by relation (3.12), we regularized equation (3.7)

at least in the unperturbed part. This known result lays the ground for introducing three orbital elements of the method proposed in this paper.

3.2 The orbital elements $\lambda_1, \lambda_2, \lambda_3$

In absence of perturbations, equation (3.13) reduces to the linear differential equation of an harmonic oscillator of unitary frequency perturbed by the constant λ_3:

$$\frac{\mathrm{d}^2 r}{\mathrm{d}\varphi^2} = -r + \lambda_3. \tag{3.16}$$

Therefore, we seek a solution of equation (3.13) in the form

$$r = \lambda_3 \left(1 - \lambda_1 \cos\varphi - \lambda_2 \sin\varphi\right), \tag{3.17}$$

$$\frac{\mathrm{d}r}{\mathrm{d}\varphi} = \lambda_3 \left(\lambda_1 \sin\varphi - \lambda_2 \cos\varphi\right), \tag{3.18}$$

where λ_1 and λ_2 are first integrals of the unperturbed motion. The two relations above imply that the following condition must be satisfied:

$$\frac{\mathrm{d}\lambda_1}{\mathrm{d}\varphi}\cos\varphi + \frac{\mathrm{d}\lambda_2}{\mathrm{d}\varphi}\sin\varphi = \frac{\varrho}{\lambda_3}\frac{\mathrm{d}\lambda_3}{\mathrm{d}\varphi}, \tag{3.19}$$

where we have introduced the quantity

$$\varrho = 1 - \lambda_1 \cos\varphi - \lambda_2 \sin\varphi. \tag{3.20}$$

Moreover, according to the VOP method we substitute the solutions (3.17) and (3.18) into equation (3.13) regarding λ_1, λ_2, λ_3 as unknown functions of φ. We obtain

$$\frac{\mathrm{d}\lambda_1}{\mathrm{d}\varphi}\sin\varphi - \frac{\mathrm{d}\lambda_2}{\mathrm{d}\varphi}\cos\varphi = (R\,r - 2\mathcal{U})\,r - \frac{\zeta}{2\,\lambda_3}\frac{\mathrm{d}\lambda_3}{\mathrm{d}\varphi}, \tag{3.21}$$

where we have set

$$\zeta = \lambda_1 \sin\varphi - \lambda_2 \cos\varphi. \tag{3.22}$$

The system of equations (3.19) and (3.21) can be solved for the derivatives of λ_1 and λ_2 to yield

$$\frac{\mathrm{d}\lambda_1}{\mathrm{d}\varphi} = (R\,r - 2\mathcal{U})\,r\,\sin\varphi + \frac{1}{2\lambda_3}\frac{\mathrm{d}\lambda_3}{\mathrm{d}\varphi}\left[(1+\varrho)\cos\varphi - \lambda_1\right], \tag{3.23}$$

$$\frac{\mathrm{d}\lambda_2}{\mathrm{d}\varphi} = (2\mathcal{U} - R\,r)\,r\,\cos\varphi + \frac{1}{2\lambda_3}\frac{\mathrm{d}\lambda_3}{\mathrm{d}\varphi}\left[(1+\varrho)\sin\varphi - \lambda_2\right]. \tag{3.24}$$

With the aid of equations (3.4), (3.10), (3.14), (3.17), and (3.18) we convert (3.15) into

$$\frac{\mathrm{d}\lambda_3}{\mathrm{d}\varphi} = 2\,\lambda_3^{5/2}\left(R_p\,\zeta\sqrt{\lambda_3} + T_p\,h + \frac{\partial\mathcal{U}}{\partial t}r\right), \tag{3.25}$$

where $R_p = \boldsymbol{P}\cdot\boldsymbol{i}$, $T_p = \boldsymbol{P}\cdot\boldsymbol{j}$. Finally, the time transformation (3.8) is conveniently rewritten as

$$\frac{\mathrm{d}t}{\mathrm{d}\varphi} = \lambda_3^{3/2}\varrho. \tag{3.26}$$

The quantities λ_1, λ_2, λ_3 are chosen as state variables of the new formulation. They determine the radial distance and the radial velocity (equations 3.17 and 3.18 together with equation 3.26) for a given value of the independent variable φ, while, in general, they are not sufficient to compute the magnitude of the angular momentum (h). In fact, from equations (3.12) and (3.14), (3.17), (3.18), we derive the formula

$$h = \sqrt{\lambda_3\left(1 - \lambda_1^2 - \lambda_2^2 - 2\mathcal{U}\,\lambda_3\varrho^2\right)}, \tag{3.27}$$

where the disturbing potential energy $\mathcal{U}$ can be a function of the position and time. To completely characterize the dynamics of the propagated body, we have to determine the physical time (Section 4) and the evolution of the unit vectors $\boldsymbol{i}$, $\boldsymbol{j}$ of the orbital frame (Section 5).

4 TIME ELEMENT

The most straightforward way to compute the physical time is to include it in the set of the state variables and to integrate equation (3.26). An other possibility is to adopt a time element, which along a Keplerian motion is constant or varies linearly with the fictitious time (Baù & Bombardelli 2014), thus reducing the instability of the time integration.

We devise here a linear and a constant time element. The former is similar to the one proposed in Stiefel & Scheifele (1971, section 18) for their regular set of elements. Let us consider the pure two-body problem, that is $\boldsymbol{P} = \boldsymbol{0}$, $\mathcal{U} = 0$. Then, the quantities λ_1, λ_2, λ_3 are constants and the integration of equation (3.26) by separation of variables yields the generalized Kepler's equation

$$t = \lambda_{0,l} + \lambda_3^{3/2}\left(\lambda_2\cos\varphi - \lambda_1\sin\varphi\right), \tag{4.1}$$

where we have defined the time element $\lambda_{0,l}$ as the sum of the constant of integration $\lambda_{0,c}$ and the term linear in φ:

$$\lambda_{0,l} = \lambda_{0,c} + \lambda_3^{3/2}\,\varphi. \tag{4.2}$$

Assuming now that the motion is perturbed we differentiate equation (4.1) and use (3.23)–(3.26) to derive

$$\frac{\mathrm{d}\lambda_{0,l}}{\mathrm{d}\varphi} = \lambda_3^{3/2}\left[1 + (R\,r - 2\mathcal{U})\,r + \frac{\zeta}{\lambda_3}\frac{\mathrm{d}\lambda_3}{\mathrm{d}\varphi}\right], \tag{4.3}$$

where ζ is given in (3.22). A constant time element can be directly defined from equation (4.2) as

$$\lambda_{0,c} = \lambda_{0,l} - \lambda_3^{3/2}\,\varphi, \tag{4.4}$$

and by exploiting (4.3) we easily compute the derivative of $\lambda_{0,c}$:

$$\frac{\mathrm{d}\lambda_{0,c}}{\mathrm{d}\varphi} = \lambda_3^{3/2}\left[(R\,r - 2\mathcal{U})\,r + \frac{1}{\lambda_3}\left(\zeta - \frac{3}{2}\varphi\right)\frac{\mathrm{d}\lambda_3}{\mathrm{d}\varphi}\right]. \tag{4.5}$$

Either $\lambda_{0,l}$ or $\lambda_{0,c}$ can be selected as one of our state variables. Use of equation (4.1) in numerical propagations is discussed in Section 6.

5 THE INTERMEDIATE FRAME

Following a similar approach to Baù & Bombardelli (2014), we define the generalized eccentricity vector as

$$\boldsymbol{g} = -\boldsymbol{i} + \boldsymbol{w}\times\boldsymbol{c}, \tag{5.1}$$

where $\boldsymbol{w}$ and $\boldsymbol{c}$ are the generalized velocity and angular momentum vectors:

$$\boldsymbol{w} = \frac{\mathrm{d}r}{\mathrm{d}t}\,\boldsymbol{i} + \frac{c}{r}\,\boldsymbol{j}, \quad \boldsymbol{c} = c\,\boldsymbol{k}, \quad c = \sqrt{h^2 + 2r^2\mathcal{U}}. \tag{5.2}$$

The magnitude of $\boldsymbol{g}$, which is computed from (5.1) and (5.2) by taking into account of (3.10) and (3.12), reads

$$g = \sqrt{1 + 2\,\varepsilon\,c^2}, \tag{5.3}$$

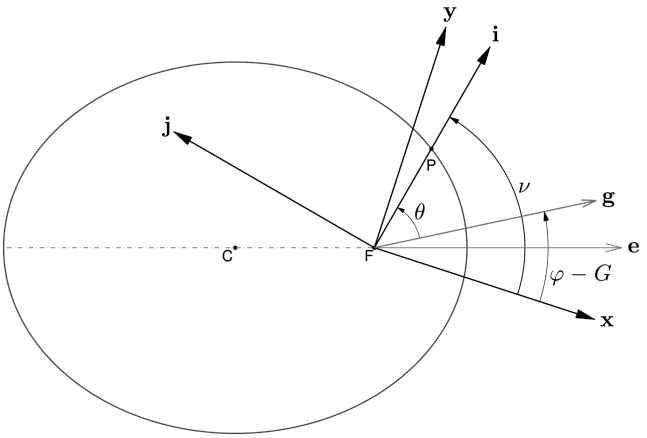

Figure 1. The intermediate frame {F; $\boldsymbol{x}$, $\boldsymbol{y}$, $\boldsymbol{k}$} as viewed from the $\boldsymbol{k}$-axis (see equation 3.3). The propagated object P occupies one point of the instantaneous osculating ellipse with centre in C and one focus in F. The generalized eccentricity vector $\boldsymbol{g}$ (equation 5.1) coincides with the osculating eccentricity vector $\boldsymbol{e}$ only if $\mathcal{U} = 0$. In the case of $\mathcal{U} \neq 0$ they share the same direction only if $\frac{\mathrm{d}r}{\mathrm{d}t} = 0$.

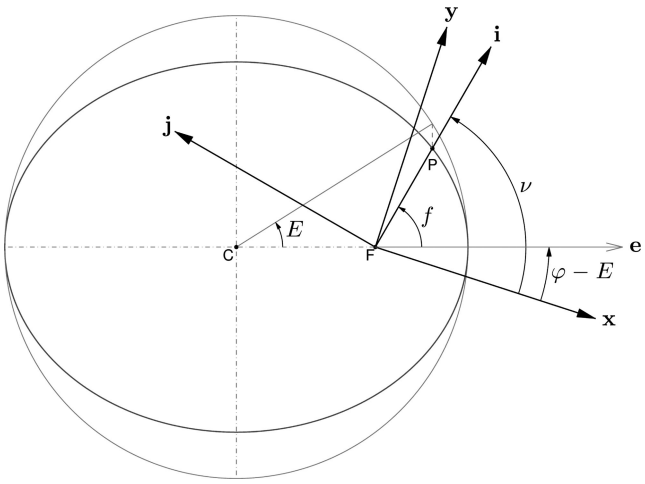

Figure 2. Same as Fig. 1 but for the case $\mathcal{U} = 0$. The angles G and θ of Fig. 1 become the osculating eccentric (E) and true (f) anomaly, respectively.

with $0 \leq g < 1$. The orientation of $\boldsymbol{g}$ on the orbital plane can be represented by the generalized true anomaly θ:

$$g\cos\theta = \frac{c^2}{r} - 1, \quad g\sin\theta = c\,\frac{\mathrm{d}r}{\mathrm{d}t}. \tag{5.4}$$

The angle θ is reckoned from $\boldsymbol{g}$ up to the radial direction $\boldsymbol{i}$ anticlockwise with respect to $\boldsymbol{k}$ (see Fig. 1).

In analogy with the definition of the osculating eccentric anomaly, we can introduce the generalized eccentric anomaly G as follows:

$$g\cos G = 1 + 2\,\varepsilon\, r, \quad g\sin G = -2\,\varepsilon\,\frac{\mathrm{d}r}{\mathrm{d}\varphi}. \tag{5.5}$$

After replacing r, $\frac{\mathrm{d}r}{\mathrm{d}\varphi}$ in equations (5.5) with the expressions given in (3.17) and (3.18), and recalling (3.14), we find for λ_1 and λ_2 these compact formulae:

$$\lambda_1 = g\,\cos(\varphi - G), \tag{5.6}$$

$$\lambda_2 = g\,\sin(\varphi - G). \tag{5.7}$$

They represent the projections of $\boldsymbol{g}$ along two orthonormal vectors, denoted by $\boldsymbol{x}$ and $\boldsymbol{y}$:

$$\boldsymbol{g} = \lambda_1\,\boldsymbol{x} + \lambda_2\,\boldsymbol{y}. \tag{5.8}$$

Next, we impose the condition $\boldsymbol{x} \times \boldsymbol{y} = \boldsymbol{k}$, where $\boldsymbol{k}$ is perpendicular to the orbital plane (see 3.3), and introduce the intermediate frame $\mathcal{I} = \{\mathrm{F}; \boldsymbol{x}, \boldsymbol{y}, \boldsymbol{k}\}$. The direction of $\boldsymbol{x}$ locates the departure point from which we measure the longitude ν of the propagated object (Fig. 1). From the definition of θ (given in 5.4) and the relations (5.6)–(5.8) we have

$$\boldsymbol{x} = \boldsymbol{i}\,\cos\nu - \boldsymbol{j}\,\sin\nu, \tag{5.9}$$

$$\boldsymbol{y} = \boldsymbol{j}\,\cos\nu + \boldsymbol{i}\,\sin\nu, \tag{5.10}$$

where the unit vectors $\boldsymbol{i}$, $\boldsymbol{j}$ belong to the orbital frame $\mathcal{O}$ (see 3.3) and

$$\nu = \varphi + \theta - G. \tag{5.11}$$

Therefore, the relative angular velocity of $\mathcal{I}$ with respect to $\mathcal{O}$ is

$$\boldsymbol{\omega}_{\mathcal{I}\mathcal{O}} = -\frac{\mathrm{d}\nu}{\mathrm{d}t}\,\boldsymbol{k}, \tag{5.12}$$

and its absolute angular velocity results

$$\boldsymbol{\omega}_{\mathcal{I}} = \boldsymbol{\omega}_{\mathcal{O}} + \boldsymbol{\omega}_{\mathcal{I}\mathcal{O}} = N\,\frac{r}{h}\,\boldsymbol{i} + \left(\frac{h}{r^2} - \frac{\mathrm{d}\nu}{\mathrm{d}t}\right)\boldsymbol{k}, \tag{5.13}$$

where N and $\boldsymbol{\omega}_{\mathcal{O}}$ are given in (3.5) and (3.6). For later reference, let us introduce

$$\boldsymbol{\omega} = \frac{\mathrm{d}t}{\mathrm{d}\varphi}\,\boldsymbol{\omega}_{\mathcal{I}}. \tag{5.14}$$

As will be clear once we provide the expression for $\frac{\mathrm{d}\nu}{\mathrm{d}\varphi}$ (equation 5.20), the intermediate frame $\mathcal{I}$ is not an ideal frame (according to the definition of Deprit 1976) since the component of the angular velocity $\boldsymbol{\omega}_{\mathcal{I}}$ along $\boldsymbol{k}$ is not identically zero. Besides, the attitude of $\mathcal{I}$ is influenced, in general, not only by N, as for the ideal frames developed in Deprit (1975) and Peláez et al. (2007), but also by the in-plane projections of $\boldsymbol{F}$ (i.e. R and T, see 3.5).

The intermediate frame has a simple geometrical interpretation if the disturbing potential energy $\mathcal{U}$ is zero (Fig. 2). In this case, the generalized quantities introduced so far convert into their osculating counterparts. Hence, at a given epoch, G is the osculating eccentric anomaly and $\varphi - G$ represents the angular separation between the unit vector $\boldsymbol{x}$ and the osculating eccentricity vector $\boldsymbol{e}$.

5.1 The orbital elements λ_4, λ_5, λ_6, λ_7

The orbital basis $\{\boldsymbol{i}, \boldsymbol{j}, \boldsymbol{k}\}$ can be determined from the longitude ν and the attitude of the intermediate basis $\{\boldsymbol{x}, \boldsymbol{y}, \boldsymbol{k}\}$ by applying relations (5.9) and (5.10).

We show in Appendix A that the angle ν (equation 5.11) is the following function of λ_1, λ_2, λ_3, and φ:

$$\nu = \varphi + 2\,\arctan\left(\frac{\zeta}{\sqrt{1 - \lambda_1^2 - \lambda_2^2 + \varrho}}\right), \tag{5.15}$$

where ϱ and ζ were defined in equations (3.20) and (3.22). As concerns the intermediate frame $\mathcal{I}$, we select four Euler parameters,

denoted by $\boldsymbol{\lambda} = (\lambda_4, \lambda_5, \lambda_6, \lambda_7)^T$ to represent its attitude in space. The evolution of $\boldsymbol{\lambda}$ is governed by the differential equation

$$\frac{\mathrm{d}\boldsymbol{\lambda}}{\mathrm{d}\varphi} = \frac{1}{2}\begin{pmatrix} 0 & \omega_z & -\omega_y & \omega_x \\ -\omega_z & 0 & \omega_x & \omega_y \\ \omega_y & -\omega_x & 0 & \omega_z \\ -\omega_x & -\omega_y & -\omega_z & 0 \end{pmatrix}\boldsymbol{\lambda}, \tag{5.16}$$

where ω_x, ω_y, ω_z are the projections of the angular velocity $\boldsymbol{\omega}$ (equation 5.14) along the axes of $\mathcal{I}$:

$$\omega_x = \boldsymbol{\omega}\cdot\boldsymbol{x} = N\,\frac{r^2}{n}\,\cos\nu, \tag{5.17}$$

$$\omega_y = \boldsymbol{\omega}\cdot\boldsymbol{y} = N\,\frac{r^2}{n}\,\sin\nu, \tag{5.18}$$

$$\omega_z = \boldsymbol{\omega}\cdot\boldsymbol{k} = \frac{n}{\varrho} - \frac{\mathrm{d}\nu}{\mathrm{d}\varphi}, \tag{5.19}$$

being $n = \frac{h}{\sqrt{\lambda_3}}$ with h given in (3.27). In equations (5.17) and (5.18) the longitude ν takes the expression shown in equation (5.15). Moreover, the derivative $\frac{\mathrm{d}\nu}{\mathrm{d}\varphi}$ in (5.19) is provided by the formula (the derivation is detailed in Appendix A)

$$\frac{\mathrm{d}\nu}{\mathrm{d}\varphi} = \frac{m}{\varrho} + \frac{1}{m\,(1+m)}\left[(2\mathcal{U} - R\,r)\,(\varrho - m - 2)\,r + \frac{\zeta\,(m-\varrho)}{2\,\lambda_3}\,\frac{\mathrm{d}\lambda_3}{\mathrm{d}\varphi}\right], \tag{5.20}$$

where R is the radial component of the perturbing force vector (see 3.5) and m is the auxiliary variable reported in (6.11). Note that in the case of Keplerian motion we have $\boldsymbol{\omega} = \mathbf{0}$ and from (5.16) the four Euler parameters in $\boldsymbol{\lambda}$ are constants. We choose λ_i, $i = 4\ldots 7$, as the remaining state variables of our formulation. In the next subsection, we will show that these elements can be generated by following a completely different approach, which relies on a new set of linear differential equations of the unperturbed two-body problem.

5.2 Alternative derivation

Let us rotate the orbital frame (see 3.3) around the direction of $\boldsymbol{k}$ by the angle $\theta - G$, where the generalized anomalies θ and G were introduced in (5.4) and (5.5), respectively, and define the vectors

$$\boldsymbol{x}^* = \boldsymbol{i}\,\cos(\theta - G) - \boldsymbol{j}\,\sin(\theta - G), \quad \boldsymbol{y}^* = \boldsymbol{k}\times\boldsymbol{x}^*. \tag{5.21}$$

Noting that $\theta - G = \nu - \varphi$ (see equation 5.11) and recalling the meaning of $\boldsymbol{\omega}$ (equation 5.14), the angular velocity vector of the frame $\mathcal{I}^* = \{\mathrm{F}; \boldsymbol{x}^*, \boldsymbol{y}^*, \boldsymbol{k}\}$ in the fictitious time φ can be written as $\boldsymbol{\omega}^* = \boldsymbol{\omega} + \boldsymbol{k}$. Along a Keplerian orbit we have $\boldsymbol{\omega}^* = \boldsymbol{k}$, so that

$$\frac{\mathrm{d}\boldsymbol{x}^*}{\mathrm{d}\varphi} = \boldsymbol{y}^*, \quad \frac{\mathrm{d}\boldsymbol{y}^*}{\mathrm{d}\varphi} = -\boldsymbol{x}^*, \tag{5.22}$$

and each component of the unit vector $\boldsymbol{x}^*$ is the solution of an harmonic oscillator of frequency equal to one. Equations (3.16), (5.22), and

$$\frac{\mathrm{d}\lambda_{0,l}}{\mathrm{d}\varphi} = \lambda_3^{3/2}, \quad \frac{\mathrm{d}\lambda_3}{\mathrm{d}\varphi} = 0, \tag{5.23}$$

($\lambda_{0,c}$ can be taken instead of $\lambda_{0,l}$) form a tenth-order linear system whose solutions are Lyapunov stable, and which is equivalent to the non-linear equation (3.2) when $\boldsymbol{F} = \mathbf{0}$. The system represented by equations (3.16) and (5.22) is analogous to the one derived by Burdet (1969) for the inverse orbital radius and the radial unit vector, and, as far as we know, has never been presented before. Then, we consider four Euler parameters $\boldsymbol{\lambda}^* = (\lambda_4^*, \lambda_5^*, \lambda_6^*, \lambda_7^*)^T$ linked with the frame $\mathcal{I}^*$. Along a Keplerian orbit $\boldsymbol{\lambda}^*$ obeys the linear differential equation

$$\frac{\mathrm{d}\boldsymbol{\lambda}^*}{\mathrm{d}\varphi} = \frac{1}{2}\begin{pmatrix} 0 & 1 & 0 & 0 \\ -1 & 0 & 0 & 0 \\ 0 & 0 & 0 & 1 \\ 0 & 0 & -1 & 0 \end{pmatrix}\boldsymbol{\lambda}^*, \tag{5.24}$$

and its solution reads

$$\begin{pmatrix} \lambda_4^* \\ \lambda_5^* \\ \lambda_6^* \\ \lambda_7^* \end{pmatrix} = \cos\frac{\varphi}{2}\begin{pmatrix} \lambda_4 \\ \lambda_5 \\ \lambda_6 \\ \lambda_7 \end{pmatrix} - \sin\frac{\varphi}{2}\begin{pmatrix} \lambda_5 \\ -\lambda_4 \\ \lambda_7 \\ -\lambda_6 \end{pmatrix}, \tag{5.25}$$

where λ_i, $i = 4\ldots 7$, are constants of integration. Equations (5.25) reveal that such constants are Euler parameters associated with a certain frame $\mathcal{I}$, and that a rotation of φ around $\boldsymbol{k}$ brings $\mathcal{I}$ to coincide with $\mathcal{I}^*$. Therefore, from equations (5.9)–(5.11) and (5.21) we infer that $\mathcal{I}$ is the intermediate frame $\{\mathrm{F}; \boldsymbol{x}, \boldsymbol{y}, \boldsymbol{k}\}$ and so the quantities λ_i, $i = 4\ldots 7$, are the orbital elements employed in our method. A final remark concerns equation (5.24): to our knowledge, linear differential equations of Euler parameters in the two-body problem have never been obtained with a classical Sundman transformation of the physical time (i.e. linear in the orbital radius).

6 IMPLEMENTATION OF THE METHOD

The method consists of a time element and seven spatial elements. Four Euler parameters track the evolution of an intermediate frame, which, in analogy to Hansen's ideal frame (Deprit 1975), specifies the orientation of the orbital plane and of a reference direction on it ($\boldsymbol{x}$), called departure point. Other three elements together with the independent variable fix the angle between $\boldsymbol{x}$ and the radial unit vector $\boldsymbol{i}$, and characterize the motion along $\boldsymbol{i}$. The last missing information is about the magnitude of the angular momentum. In general, this is a function of the whole set of elements through the disturbing potential energy $\mathcal{U}$ (see equation 3.27).

In this section, we write the eight differential equations in a suitable form to the implementation in a computer program. Then, we show how to pass from the orbital elements to the position and velocity and vice versa, since these are necessary operations in a numerical propagation.

6.1 Differential equations

We collect below the differential equations of the eight variables of the new method (equations 4.3, 3.23, 3.24, 3.25, 5.16):

$$\frac{\mathrm{d}\lambda_{0,l}}{\mathrm{d}\varphi} = \lambda_3^{3/2}\,[1 + (R\,r - 2\mathcal{U})\,r + 2\,\Lambda_3\,\zeta], \tag{6.1}$$

$$\frac{\mathrm{d}\lambda_1}{\mathrm{d}\varphi} = (R\,r - 2\mathcal{U})\,r\,\sin\varphi + \Lambda_3\left[(1+\varrho)\cos\varphi - \lambda_1\right], \tag{6.2}$$

$$\frac{\mathrm{d}\lambda_2}{\mathrm{d}\varphi} = (2\mathcal{U} - R\,r)\,r\,\cos\varphi + \Lambda_3\left[(1+\varrho)\sin\varphi - \lambda_2\right], \tag{6.3}$$

$$\frac{\mathrm{d}\lambda_3}{\mathrm{d}\varphi} = 2\,\lambda_3^3\left(R_p\,\zeta + T_p\,n + \frac{\partial\mathcal{U}}{\partial t}\,\sqrt{\lambda_3}\varrho\right), \tag{6.4}$$

$$\frac{\mathrm{d}}{\mathrm{d}\varphi}\begin{pmatrix}\lambda_4\\ \lambda_5\\ \lambda_6\\ \lambda_7\end{pmatrix} = N\,\frac{r^2}{2\,n}\begin{pmatrix}\lambda_7\,c_\nu - \lambda_6\,s_\nu\\ \lambda_6\,c_\nu + \lambda_7\,s_\nu\\ -\lambda_5\,c_\nu + \lambda_4\,s_\nu\\ -\lambda_4\,c_\nu - \lambda_5\,s_\nu\end{pmatrix} + \frac{\omega_z}{2}\begin{pmatrix}\lambda_5\\ -\lambda_4\\ \lambda_7\\ -\lambda_6\end{pmatrix}, \quad (6.5)$$

where (equations 3.17, 5.15, 5.19, 5.20)

$$r = \lambda_3\varrho, \quad (6.6)$$

$$c_\nu = \cos\nu, \quad s_\nu = \sin\nu, \quad \nu = \varphi + 2\arctan\left(\frac{\zeta}{m+\varrho}\right), \quad (6.7)$$

$$\omega_z = \frac{n-m}{\varrho} + \frac{1}{m\,(1+m)}\left[(2\,\mathcal{U} - R\,r)\,(2-\varrho+m)\,r + \Lambda_3\,\zeta\,(\varrho-m)\right], \quad (6.8)$$

and

$$\Lambda_3 = \frac{1}{2\lambda_3}\,\frac{\mathrm{d}\lambda_3}{\mathrm{d}\varphi}, \quad (6.9)$$

$$\varrho = 1 - \lambda_1\cos\varphi - \lambda_2\sin\varphi, \quad \zeta = \lambda_1\sin\varphi - \lambda_2\cos\varphi, \quad (6.10)$$

$$n = \sqrt{m^2 - 2\,\lambda_3\varrho^2\,\mathcal{U}}, \quad m = \sqrt{1-\lambda_1^2-\lambda_2^2}. \quad (6.11)$$

Since ν appears only as argument of trigonometric functions, it is possible to avoid equation (6.7) and directly employ the expressions

$$\varrho c_\nu = \cos\varphi - \lambda_1 + \frac{\zeta\lambda_2}{m+1}, \quad \varrho s_\nu = \sin\varphi - \lambda_2 - \frac{\zeta\lambda_1}{m+1}. \quad (6.12)$$

Moreover, given the perturbing force $\boldsymbol{F}$ (equation 3.2) we have

$$R = \boldsymbol{F}\cdot\boldsymbol{i}, \quad N = \boldsymbol{F}\cdot\boldsymbol{k}, \quad R_p = \boldsymbol{P}\cdot\boldsymbol{i}, \quad T_p = \boldsymbol{P}\cdot\boldsymbol{j}, \quad (6.13)$$

where $\boldsymbol{i}$, $\boldsymbol{j}$, $\boldsymbol{k}$ are obtained as shown in Section 6.2. Note that we report only the differential equation of the linear time element $\lambda_{0,l}$ (equation 6.1), but one may employ instead $\lambda_{0,c}$ (equation 4.5) or the physical time (equation 3.26).

The system (6.1)–(6.5) holds for negative values of the total energy (ε). Additionally, we require that the potential $\mathcal{U}(t, \boldsymbol{r})$ satisfies $c^2 > 0$, where c is the generalized angular momentum (see 5.2; this issue is discussed in Baù et al. 2013, section 6). The conditions $\varepsilon < 0$ and $c \neq 0$ imply that $(0 \leq)\ g < 1$ (see equation 5.3), and, since $m^2 = 1 - g^2$ (from equations 5.6, 5.7, 6.11), we have in particular $m \neq 0$, thus avoiding the singularity in (6.8). Finally, equation (6.5) become singular when $h = 0$.

Remark. In both methods presented in this work and in Baù et al. (2013) the disturbing potential energy $\mathcal{U}$ is assumed to be independent on the velocity $\boldsymbol{v}$. However, this hypothesis could be relaxed since what we really ask is that $\mathcal{U}$ is independent on the osculating angular momentum h, which enters the component of $\boldsymbol{v}$ along $\boldsymbol{j}$ (see equations 3.4, 3.27, and equation 45 in Baù et al. 2013).

6.2 Computation of the position, velocity, and time from the orbital elements and from the independent variable

The components of the unit vectors $\boldsymbol{x}, \boldsymbol{y}, \boldsymbol{k}$ of the intermediate frame along three orthonormal axes with fixed directions can be written in function of the Euler parameters λ_i, $i = 4\ldots7$, as

$$\boldsymbol{x} = 2\left(\frac{1}{2} - \lambda_5^2 - \lambda_6^2,\ \lambda_4\,\lambda_5 + \lambda_6\,\lambda_7,\ \lambda_4\,\lambda_6 - \lambda_5\,\lambda_7\right)^T, \quad (6.14)$$

$$\boldsymbol{y} = 2\left(\lambda_4\,\lambda_5 - \lambda_6\,\lambda_7,\ \frac{1}{2} - \lambda_4^2 - \lambda_6^2,\ \lambda_5\,\lambda_6 + \lambda_4\,\lambda_7\right)^T, \quad (6.15)$$

$$\boldsymbol{k} = 2\left(\lambda_4\,\lambda_6 + \lambda_5\,\lambda_7,\ \lambda_5\,\lambda_6 - \lambda_4\,\lambda_7,\ \frac{1}{2} - \lambda_4^2 - \lambda_5^2\right)^T. \quad (6.16)$$

Then, we get the radial and transverse unit vectors $\boldsymbol{i}$ and $\boldsymbol{j}$ from

$$\boldsymbol{i} = \boldsymbol{x}\,\cos\nu + \boldsymbol{y}\,\sin\nu, \quad (6.17)$$

$$\boldsymbol{j} = \boldsymbol{y}\,\cos\nu - \boldsymbol{x}\,\sin\nu, \quad (6.18)$$

where $\cos\nu$ and $\sin\nu$ are provided by equations (6.12).
The (dimensionless) position vector reads

$$\boldsymbol{r} = \lambda_3\,(1 - \lambda_1\cos\varphi - \lambda_2\sin\varphi)\,\boldsymbol{i}. \quad (6.19)$$

If a linear ($\lambda_{0,l}$), constant ($\lambda_{0,c}$) time element is employed then the (dimensionless) physical time is computed as

$$t = \lambda_{0,l} - \lambda_3^{3/2}\,(\lambda_1\sin\varphi - \lambda_2\cos\varphi), \quad (6.20)$$

$$t = \lambda_{0,c} - \lambda_3^{3/2}\,(\lambda_1\sin\varphi - \lambda_2\cos\varphi - \varphi), \quad (6.21)$$

respectively.
Finally, we get the (dimensionless) velocity vector from the relation

$$\boldsymbol{v} = v_r\,\boldsymbol{i} + v_t\,\boldsymbol{j}, \quad (6.22)$$

where the radial and transversal components are

$$v_r = \frac{\lambda_1\sin\varphi - \lambda_2\cos\varphi}{\sqrt{\lambda_3}\varrho}, \quad v_t = \sqrt{\frac{1-\lambda_1^2-\lambda_2^2}{\lambda_3\varrho^2} - 2\,\mathcal{U}}, \quad (6.23)$$

with ϱ given in (6.10).

6.3 Computation of the orbital elements from the position, velocity, and time

We assume to know the (dimensionless) physical time t, position, and velocity vectors $(\boldsymbol{r}, \boldsymbol{v})$ in the frame $\mathcal{F} = \{\mathrm{F}; \boldsymbol{e}_1, \boldsymbol{e}_2, \boldsymbol{e}_3\}$ having fixed axes in space.

The corresponding total energy and angular momentum vector are

$$\varepsilon = \frac{v^2}{2} - \frac{1}{r} + \mathcal{U}, \quad \boldsymbol{h} = \boldsymbol{r}\times\boldsymbol{v}, \quad (6.24)$$

where $r = |\boldsymbol{r}|$ and $v = |\boldsymbol{v}|$. The generalized angular momentum is given by

$$c = \sqrt{h^2 + 2\,r^2\,\mathcal{U}}, \quad (6.25)$$

with $h = |\boldsymbol{h}|$. Among the possible values of the independent variable φ we suggest ($2\,\varepsilon\,c^2 \neq -1$)

$$\varphi = G = \mathrm{atan2}\left(\boldsymbol{r}\cdot\boldsymbol{v}\,\sqrt{-2\,\varepsilon},\ 1 + 2\,\varepsilon\,r\right), \quad (6.26)$$

where G is the generalized eccentric anomaly (equation 5.5). This choice implies (equations 5.3, 5.6, 5.7)

$$\lambda_1 = \sqrt{1 + 2\,\varepsilon\,c^2}, \quad \lambda_2 = 0. \quad (6.27)$$

For a generic value of φ the elements λ_1 and λ_2 are calculated through the formulae

$$\lambda_1 = (1 + 2\,\varepsilon\,r)\cos\varphi + \boldsymbol{r}\cdot\boldsymbol{v}\,\sqrt{-2\,\varepsilon}\,\sin\varphi, \quad (6.28)$$

$$\lambda_2 = (1 + 2\,\varepsilon\,r)\sin\varphi - \boldsymbol{r}\cdot\boldsymbol{v}\,\sqrt{-2\,\varepsilon}\,\cos\varphi. \quad (6.29)$$

Moreover, we have

$$\lambda_3 = -\frac{1}{2\,\varepsilon}, \tag{6.30}$$

and the time element is recovered by

$$\lambda_{0,l} = t + \lambda_3^{3/2}\,(\lambda_1 \sin\varphi - \lambda_2 \cos\varphi)\,, \tag{6.31}$$

$$\lambda_{0,c} = t + \lambda_3^{3/2}\,(\lambda_1 \sin\varphi - \lambda_2 \cos\varphi - \varphi)\,. \tag{6.32}$$

In order to determine the remaining elements, we first compute the angle ν,

$$\nu = \varphi + 2\,\arctan\left(\frac{\boldsymbol{r}\cdot\boldsymbol{v}}{c + r\,\sqrt{-2\,\varepsilon}}\right). \tag{6.33}$$

Then, we obtain the unit vectors $\boldsymbol{x}$, $\boldsymbol{y}$, $\boldsymbol{k}$ of the intermediate frame:

$$\boldsymbol{x} = \boldsymbol{i}\,\cos\nu - \boldsymbol{j}\,\sin\nu, \quad \boldsymbol{y} = \boldsymbol{j}\,\cos\nu + \boldsymbol{i}\,\sin\nu, \quad \boldsymbol{k} = \frac{\boldsymbol{h}}{h}, \tag{6.34}$$

where

$$\boldsymbol{i} = \frac{\boldsymbol{r}}{r}, \quad \boldsymbol{j} = \boldsymbol{k}\times\boldsymbol{i}. \tag{6.35}$$

Finally, from the components of $\boldsymbol{x}$, $\boldsymbol{y}$, $\boldsymbol{k}$ in the fixed frame $\mathcal{F}$ we can express the quantities λ_4, λ_5, λ_6, λ_7 by the relations

$$\lambda_7 = \frac{1}{2}\sqrt{1 + x_1 + y_2 + k_3}, \tag{6.36}$$

$$\lambda_4 = \frac{y_3 - k_2}{4\,\lambda_7}, \quad \lambda_5 = \frac{k_1 - x_3}{4\,\lambda_7}, \quad \lambda_6 = \frac{x_2 - y_1}{4\,\lambda_7}, \tag{6.37}$$

where, for a generic vector $\boldsymbol{a}$, we mean $a_\alpha = \boldsymbol{a}\cdot\boldsymbol{e}_\alpha$, $\alpha = 1, 2, 3$. The singular case $\lambda_7 = 0$ is discussed in Appendix B.

7 NUMERICAL COMPARISONS

The method presented in the previous sections is used to calculate the special perturbations of a small body orbiting around a primary body of attraction. The performance of the new formulation is compared with that of many others for three examples. The details of the numerical investigation and the comments on the results are reported below.

7.1 Formulations

Three different algorithms of the new method were implemented by combining the quantities $\lambda_1 \ldots \lambda_7$ with either the physical time or a linear, constant time element. In the numerical tests several formulations of the perturbed two-body problem were compared. Those for which the state vector is made only by orbital elements are (see Table 1): the Stiefel–Scheifele regular variables (Stiefel & Scheifele 1971, section 19); Stiefel's spatial elements (Stiefel et al. 1967, p. 18) completed by a constant time element (Arakida & Fukushima 2001, appendix); a new version of Stiefel's elements (named Stiefel*) provided with a constant, linear time element (see Appendix C); Dromo(PC) and Dromo(PL) (Baù & Bombardelli 2014). We included also the method Dromo(P) (Baù et al. 2013), in which the physical time is a state variable. Two versions of each Dromo scheme were coded depending on whether the total energy (ε, see equation 3.9) or the generalized angular momentum (c, see 5.2) is adopted as one of the state variables. The following methods that rely mainly on coordinates (see Table 1) are considered: the Kustaanheimo-Stiefel regularization (Stiefel & Scheifele 1971, section 9); the stabilized Cowell's method invented by Baumgarte (1972), with or without a time element (the former version was tested by Janin 1974); different implementations of the Burdet–Ferrándiz (B–F) regularization. More specifically, we tested the B–F method as it is reported in appendix C.2 of Fukushima (2007a), and

Table 1. Formulations included in the numerical tests (a brief description is reported in Section 7.1). The independent variable is denoted by s and the physical time by t. The quantities r, h, c, and ε are the orbital radius, the osculating angular momentum, the generalized angular momentum (see 5.2), and the total energy. In the performance plots the labels Dromo(P), Dromo(PC), Dromo(PL) are followed by either c or e to inform that $\frac{1}{c}$ and ε, respectively, is a state variable. The same notation is applied to the labels BF*, BF*(C), BF*(L) to indicate the use of c and ε in the state vector.

Formulations	Independent variable	Dim.[a]	Time	Time element: Constant	Time element: Linear
Based on orbital elements					
New	(♭) $\sqrt{-2\,\varepsilon}\,\mathrm{d}t = r\,\mathrm{d}s$	8	x		
New(C)	(♭)	8		x	
New(L)	(♭)	8			x
Sti&Sche	(♭)	10			x
Stiefel(C)	(♮) $\mathrm{d}t = r\,\mathrm{d}s$	10		x	
Stiefel*(C)	(♮)	10		x	
Stiefel*(L)	(♮)	10			x
Dromo(P)	(♯) $c\,\mathrm{d}t = r^2\,\mathrm{d}s$	8	x		
Dromo(PC)	(♯)	8		x	
Dromo(PL)	(♯)	8			x
Based on coordinates					
KS	(♮)	10			x
CowS	(♮)	8	x		
CowS(L)	(♮)	8			x
BF	$h\,\mathrm{d}t = r^2\,\mathrm{d}s$	10	x		
BF*	(♯)	10	x		
BF*(C)	(♯)	10		x	
BF*(L)	(♯)	10			x

[a]This is the dimension of the state vector.

the modified version (named BF*) shown in Appendix C, where a constant and a linear time element are also supplied. For BF*, BF*(C), BF*(L) we took into account the possibility of employing the total energy as a state variable instead of the element c. Table 1 contains some relevant details of all these formulations, which will be referred to as indicated in the first column of this table.

7.2 Numerical integrators

The formulations of the previous subsection were paired to a single-step and a multistep numerical integrator (Henrici 1962). Among the one-step methods we selected the Runge–Kutta (4, 5) pair of Dormand & Prince (1980), hereafter called DOPRI54, as coded in the MATLAB function ode45.m. An important feature is that the length of the step size is controlled by relative and absolute tolerances. One multistep method that we used for the numerical tests consists in the Adams–Bashforth and the Adams–Moulton formulae in the summed form (Montenbruck & Gill 2000, equations 4.95 and 4.96) implemented in a PECE (predict, evaluate, correct, evaluate) scheme. This algorithm, which will be referred to as ABM, and the DOPRI54, can be applied to any formulation in Table 1. The methods based on coordinates were also combined with an other multistep integrator. For these schemes the state vector takes the form $\left(\boldsymbol{q};\boldsymbol{q}';z\right)$, where $\boldsymbol{q}' = \frac{\mathrm{d}\boldsymbol{q}}{\mathrm{d}s}$ and s is the independent variable. The vector $\boldsymbol{q}$ is governed by a second-order differential equation and its propagation is carried out by Störmer's and Cowell's methods of order p in PECE mode. Secund-sum formulae, known as Gauss–Jackson methods, are employed (Montenbruck & Gill 2000, equations 4.93 and 4.94). The variables contained in z and $\boldsymbol{q}'$ obey first-order differential equations and are obtained by the ABM method of order p and $p-1$, respectively. We call this multistep algorithm SC-ABM. Both the ABM and SC-ABM integrators employ a fixed step size. Finally, the starting values are provided by an implicit Runge–Kutta method of order p based on Gaussian quadrature formulae (see Hairer, Nørsett & Wanner 2009, vol. 1, p. 208, and references therein).

7.3 Performance metrics

Let us call propagator the combination of a formulation and a numerical integrator. In order to evaluate its performance, we resort to two numerical tests. The first one measures the computational cost required to achieve a certain level of accuracy. The motion is propagated from some given initial conditions until the physical time (which is not the independent variable for any of the selected formulations) reaches the desired value t_{ref}. If the position of the object is known at the time t_{ref}, and for sufficiently short propagations, we can take the distance between the computed and the reference positions as a measure of the achieved accuracy. The computational cost is represented by the total number of evaluations of the right-hand side of the differential equations (functions calls) for the DOPRI54, and by the total number of steps for the ABM and SC-ABM. By changing the step length in the multistep methods and the tolerances of the DOPRI54, which in turn control the number of function calls, we can explore the behaviour of a specific propagator. The correct position at t_{ref} is assessed as follows. Accurate propagations are carried out with a subset of formulations and the DOPRI54 integrator setting the absolute[5] and relative tolerances to a sufficiently small value (10^{-13}). Then, the common figures in each component of the final position vectors constitute the reference position. In one of the proposed examples (Example 3), the computational cost is also measured by the time spent to propagate the state vector from the initial to the final epoch.

The second performance metric is the accumulation of the error in position, time, and possible conserved quantities over a few thousand nominal periods around the primary body. With nominal period, we mean the period of the initial osculating orbit of the propagated object. The numerical integrators used in this test are the multistep methods ABM, SC-ABM, and the error is calculated with the same procedure outlined in section 3.3 of Baù & Bombardelli (2014). We will show the error obtained by a moving average filter with a window size of $N+1$, where N is the number of steps per nominal period.

7.4 Examples and results

An example is given by the initial conditions of the propagated object relative to a primary body, and by the model of the perturbations. In general, for a certain example we carry out the two numerical tests described in the previous subsection with all the available propagators. In the first test, we compare separately the results produced by the one-step and the multistep methods. Each formulation based on coordinates is combined with both the ABM and the SC-ABM, and the better behaviour of the two pairs is considered. Apart from Sti&Sche and KS, the other schemes can be divided into five groups (Table 1). Only the most efficient propagator of each group is shown in the following plots.

We propose three examples: the first two present simplified models of weak and moderate gravitational perturbations, respectively; the third one describes a more realistic scenario of motion around the Earth including also non-gravitational forces.

7.4.1 Example 1

The asteroid 1566 Icarus is propagated under the perturbation of Jupiter. The initial conditions of Icarus and Jupiter are expressed by the classical orbital elements reported in Table 2. The values are taken from Fukushima (2007b) with the exception of Jupiter's eccentricity, which is assumed to be zero. Since Jupiter is influenced only by the gravity of the Sun we have a restricted circular three-body problem and thereby the conservation of the Jacobi constant. This example represents the case of a weak perturbation: the mean value of the ratio between the accelerations exerted by Jupiter and the Sun is of the order of 10^{-4}.

Fig. 3 shows the average errors in position, time, and Jacobi constant over an interval of the independent variable corresponding to ten thousand nominal periods along Icarus' initial osculating orbit. A similar test is reported in Fukushima (2004a,b) where the author plots the error in the mean longitude at epoch. The third-body perturbation due to Jupiter is an explicit function of the physical time and is here regarded as the force $\boldsymbol{P}$ in equation (3.2). Note that the disturbing potential energy is zero in this case and so the

Table 2. Initial Keplerian elements of Icarus and Jupiter referred to the heliocentric ecliptic coordinate system at epoch J2000.0.

	a (au)	e	i (°)	Ω (°)	ω (°)	M_0 (°)
Icarus	1.078	0.827	22.9	88.1	31.3	323.8
Jupiter	5.2026	0.0	1.303	100.471	14.337	95.752

[5] In this work, we always assign the same value of the absolute tolerance to all the components of the state vector.

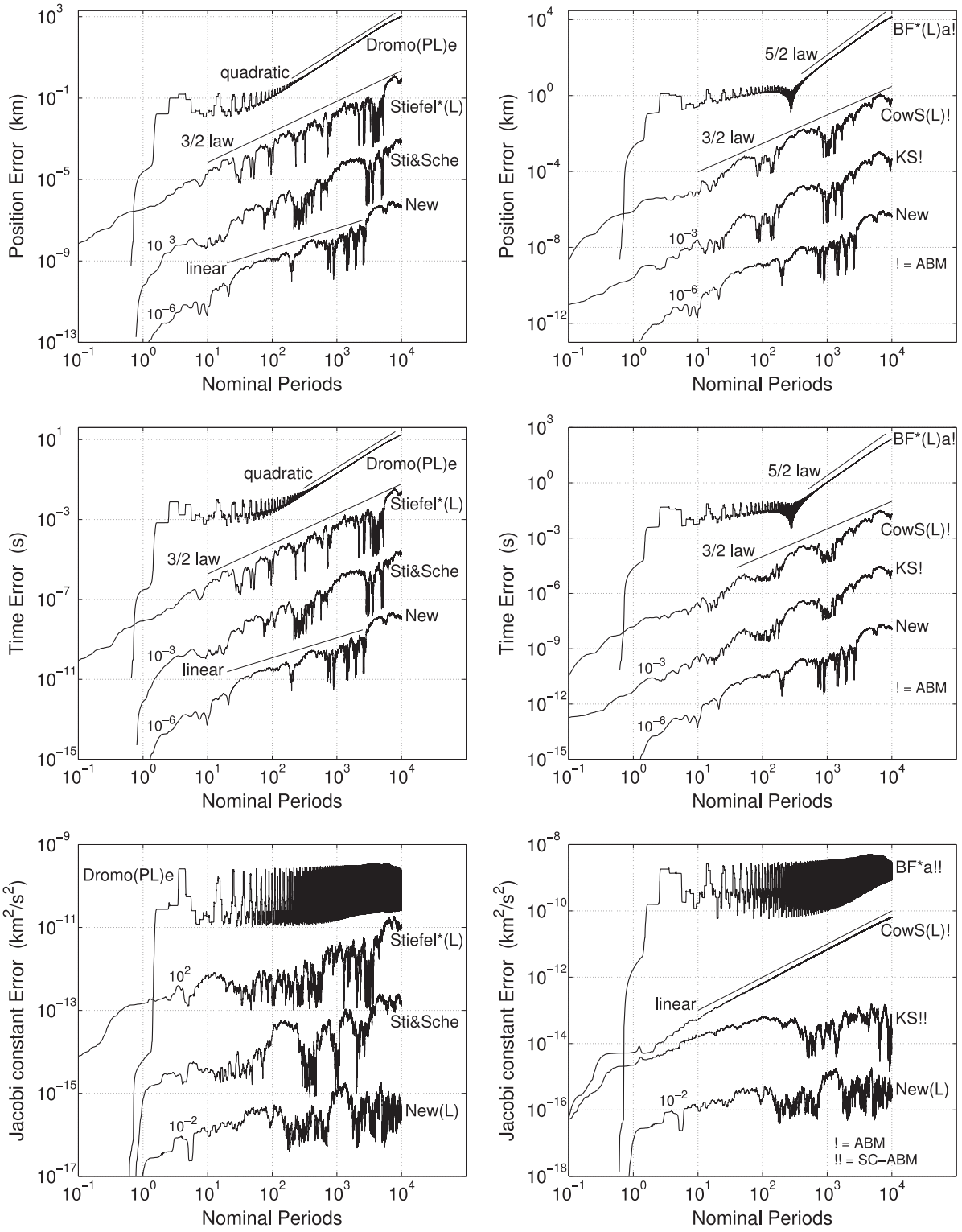

Figure 3. Position, time, and Jacobi constant error accumulated during 10000 nominal periods; example 1: Icarus perturbed by Jupiter. The new method is compared with the formulations based on elements (left-hand) and on coordinates (right-hand). The numerical integrators are the 10th-order multistep methods ABM, SC-ABM, and the number of steps per nominal period is 90. To avoid superpositions, the curves are shifted along the vertical axis by a suitable power of 10 when necessary.

formulations Stiefel*(C) and BF* in Table 1 are equivalent to Stiefel(C) and BF, respectively.

A first consideration rising from Fig. 3 is that the formulations employing a time transformation of order two (i.e. quadratic in the orbital radius, see Table 1) show the worse performance. All the other methods use time transformations linear in the orbital radius, and accumulate almost the same amount of error in position, which is of the order of 1 km at the end of the propagation. However, only

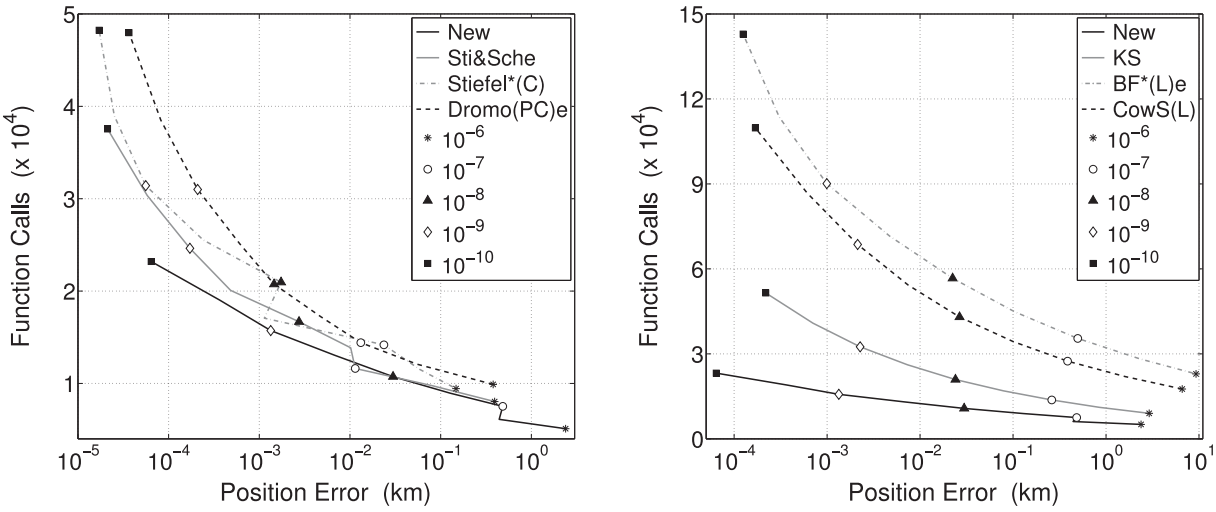

Figure 4. Function calls versus position error after 288.12768941 msd (about 49.5 revolutions); example 2: artificial satellite of the Earth perturbed by J_2, Moon. The numerical integrator is the 5th-order explicit Runge–Kutta method (DOPRI54). The relative tolerance is changed from 10^{-6} to 10^{-10}, and the absolute tolerance is set to 10^{-13}. The new method is compared with the formulations based on elements (left-hand) and on coordinates (right-hand).

New exhibits a linear growth, in the range between 10 and 3000 nominal periods. The evolutions of the time and position errors are very similar to each other for all the propagators, thus indicating how an accurate prediction of the physical time is mandatory to improve the performance of regularized formulations (Baù & Bombardelli 2014). In Fig. 3, we also display the difference between the Jacobi constant computed at each integration step and the nominal value obtained from the initial conditions. We advise that, in general, monitoring only the conservation of one integral of the motion (when it exists) is not sufficient for ranking different formulations, but can be useful to reveal further characteristics of the error. For example, the linear growth of CowS(L) suggests that a faster deterioration of the position accuracy will occur beyond the considered range of propagation with respect to KS and New, which instead exhibit an almost constant trend. In conclusion, the new method enjoys the most favourable behaviour of the error so that an increasing advantage with respect to the other methods is expected for numerical integrations longer than ten thousand nominal periods.

7.4.2 Example 2

The initial position and velocity of an artificial satellite with respect to the geocentric equatorial coordinate system ($\mathcal{F}$) are

$$\begin{aligned} \boldsymbol{r} &= (0, -5888.9727, -3400)^T \text{ km}, \\ \boldsymbol{v} &= (10.691338, 0, 0)^T \text{ km s}^{-1}. \end{aligned} \tag{7.1}$$

The eccentricity and inclination of the Keplerian orbit are about 0.95° and 30°, and the spacecraft occupies the perigee at a distance of 6800 km from the Earth's centre of mass. Two perturbations are active: the Moon's gravitational attraction and the Earth's oblateness. The former is included in the force denoted by $\boldsymbol{P}$ in equation (3.2), while for the latter we introduce the disturbing potential containing the zonal harmonic J_2. This example was invented by Stiefel & Scheifele (1971, p. 118) to test their set of regular elements. Moreover, it was considered for numerical experiments in Baù & Bombardelli (2014) and Baù et al. (2013) where one can find the formulae to implement the perturbing forces and the values of the related constants.

In the first test, we investigate the relation between the accuracy in the position at a given epoch and the computational cost. Let us pick as reference time 288.12768941 mean solar days (msd) elapsed from the initial epoch (as in the examples 2a and 2b of Stiefel & Scheifele 1971, p. 122), which corresponds to a final position close to the farthest point from the Earth of the 50th revolution. Assume that the correct coordinates of the satellite in the reference frame $\mathcal{F}$ are given by[6]

$$\boldsymbol{r}_{\text{ref}} = (-24219.0501, -227962.10637, 129753.44240)^T \text{ km}. \tag{7.2}$$

This vector is taken from table 2 of Baù et al. (2013) and it was obtained as described in Section 7.3 by employing the methods Dromo(P)a, Dromo(P)e, Sti&Sche, and the set of elements of Sperling–Burdet (Bond & Allman 1996, chapter 9). Fig. 4 displays the variation in the position error as the relative tolerance of the numerical integrator DOPRI54 is modified inside a suitable range thus producing a consequent variation of the number of function calls. In the case of the multistep methods ABM, SC-ABM (Fig. 5) we increase the number of steps per revolution starting from the minimum quantity that does not lead to numerical instability.[7] The proposed method is the most efficient both with a variable and a fixed step-size integrator, since it requires, in general, the smallest computational effort for a given accuracy.

The performance in a long-term propagation, here of five thousand nominal periods, is shown in Fig. 6. Dromo(PL)e and BF*(L)e exhibit a huge initial jump of the error in position and time followed by a quadratic growth. The errors produced by the new method remain almost constant in the first two hundred periods, then they start growing according to a 3/2 power law. It is notable that, in spite of the linear behaviour of the other formulations, New reaches the smallest amount of error at the end of the propagation. In particular, it is more accurate than KS and Sti&Sche of one and two orders of magnitude, respectively.

[6] Note that the components of the vector $\boldsymbol{r}_{\text{ref}}$ are assumed to be correct up to the shown decimal digits.

[7] Here and in the example 3, we used a minimum threshold of 32 steps per revolution.

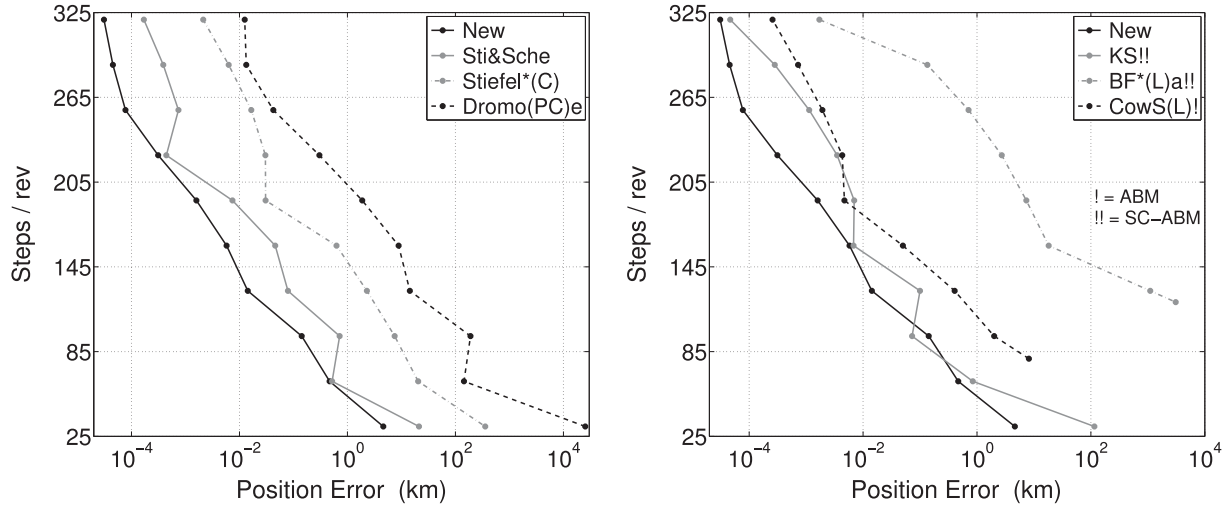

Figure 5. Number of steps per revolution versus position error after 288.12768941 msd; example 2. The numerical integrators are the 10th-order multistep methods ABM, SC-ABM. The total number of steps is given by steps/rev times 49.5.

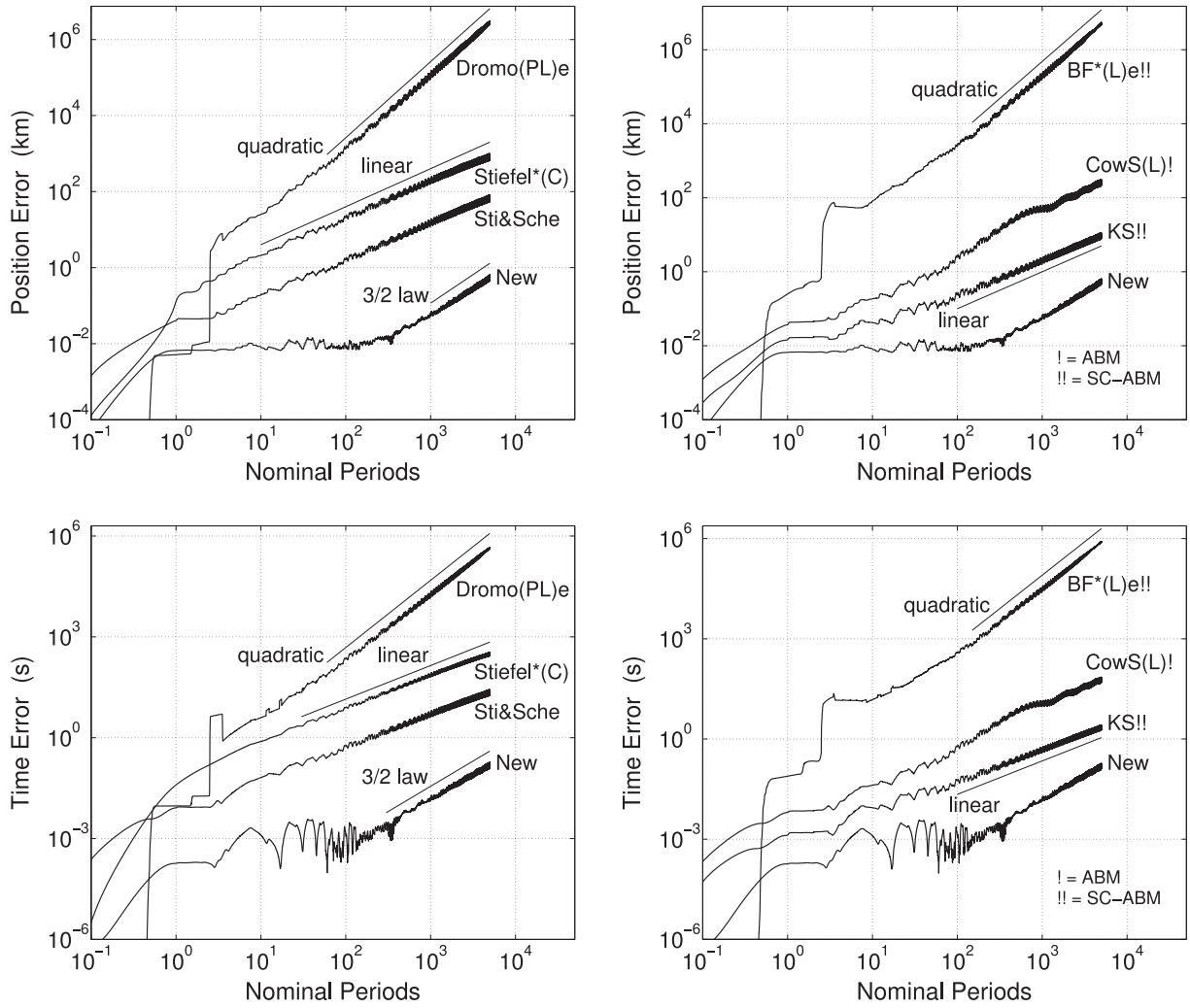

Figure 6. Position and time error accumulated during 5000 nominal periods; example 2: artificial satellite of the Earth perturbed by J_2, Moon. The new method is compared with the formulations based on elements (left-hand) and on coordinates (right-hand). The numerical integrators are the 10th-order multistep methods ABM, SC-ABM, and the number of steps per nominal period is 144.

Table 3. Reference positions (in the geocentric equatorial coordinate system) at two physical times (in mean solar days elapsed from the initial epoch) for the example 3. These values were found with the procedure described in Section 7.3 and employing the methods New, Sti&Sche, KS, CowS(L).

Time intervals (msd)	Reference positions (km)
($t_{\mathrm{ref},1}$) 288.01603946	$(-21\,572.282, 226401.054, 128\,935.148)^T$
($t_{\mathrm{ref},2}$) 291.49486175	$(-15\,477.46, -2591.82, -1936.21)^T$

7.4.3 *Example 3*

Let us consider the same initial conditions (see 7.1) and perturbations (J_2, Moon) as in the example 2, and include also the non-gravitational forces due to the direct solar radiation pressure and the atmospheric drag. The latter is implemented as described in section 7.1.3 of Baù et al. (2013). We just point out that the exponential model is adopted for the atmospheric density and the hypothesis of a compact spacecraft in free molecular flow is made. Moreover, the ratio between the cross-sectional area orthogonal to the velocity relative to the atmosphere and the spacecraft mass (m) is 0.01 m^2 kg^{-1}. As concerns the radiation pressure, we use the cannonball model and the acceleration is computed by (Milani & Gronchi 2010, p. 289)

$$\boldsymbol{P}_{\mathrm{rp}} = -\frac{\Phi}{c}\frac{\mathcal{A}}{m}\boldsymbol{s} = -P_{\mathrm{rp}}\,\boldsymbol{s}, \tag{7.3}$$

where c is the speed of light, Φ/c is the flux of momentum per unit cross-sectional area, $\mathcal{A}$ is the effective cross-sectional area, and $\boldsymbol{s}$ identifies the direction to the Sun. We assume that P_{rp} is constant and equal to 10^{-10} km s^{-2}, which is a reasonable value for an Earth satellite with an area to mass ratio of 0.01 m^2 kg^{-1} (Montenbruck & Gill 2000, p. 55). For simplicity let the Sun–spacecraft line be parallel to the Sun–Earth line. Then, if the Earth follows a circular orbit (with radius of one astronomical unit), the vector $\boldsymbol{s}$ can be written in the geocentric equatorial coordinate system $\mathcal{F}$ as

$$\boldsymbol{s} = (-\sin(w\,t), \cos(w\,t)\cos\varepsilon, \cos(w\,t)\sin\varepsilon)^T, \tag{7.4}$$

where t is the physical time, ε and w are the Earth's obliquity (we take 23.4°) and orbital angular velocity.

Let us fix two epochs such that the spacecraft is near to the apogee and perigee of the corresponding osculating orbits (see Table 3). Note that the same error in physical time produces a bigger displacement of the position in the latter case due to the faster motion. Fig. 7 shows for the two considered time intervals the position error and the function calls as the relative tolerance of the numerical integrator DOPRI54 is gradually decreased. We found that the formulations relying on orbital elements have comparable efficiency, and, in general, they outperform the methods based on coordinates. A desirable feature of our scheme is that it involves a low computational cost also for very accurate propagations (see Table 4). A linear time element proves to be beneficial in this sense, and we see that New(L) requires 2, 3, and 7 times less evaluations of the right-hand side than the Stiefel–Scheifele elements, the KS regularization, and the stabilized Cowell's method, respectively.

Next, we analyse the efficiency of the formulations paired with a multistep method. In this case we shorten the step size starting from a maximum length which is determined by applying the same criterion of the example 2. Tables 5 and 6 summarize the results for the two time intervals $t_{\mathrm{ref},1}$ and $t_{\mathrm{ref},2}$ of Table 3. As long as the number of steps per revolution (steps/rev) is sufficiently low (for example 160) the methods exploiting a classical Sundman transformation are much more accurate. However, we observe that they encounter a sort of accuracy barrier which prevents a substantial improvement passing from 320 to 640 steps/rev. On the other hand, by doubling the number of integration steps the error is progressively reduced in Dromo(PC)e, BF*(L)a, BF*a, and for 640 steps/rev it becomes two orders of magnitude smaller with respect to the other methods. These different behaviours can be explained by the fact that in time transformations of the form $\mathrm{d}t = \alpha\, r^n\, \mathrm{d}s$ ($\alpha \in \mathbb{R}^+$, $n \in \mathbb{Z}^+$) the choice $n = 2$ against $n = 1$ produces a denser distribution of points near the Earth, especially if the eccentricity is high, and thereby allows a better propagation in the region where the atmospheric drag is active. Considering the computational time spent during the integration (Table 5), we can state that in the example 3 and for short-term propagations Dromo(PC)e achieves the highest accuracy with the smallest effort if we employ a fixed step-size multistep method.

Finally, the evolution of the position error until five thousand nominal periods is shown in Fig. 8. As we expected the error is

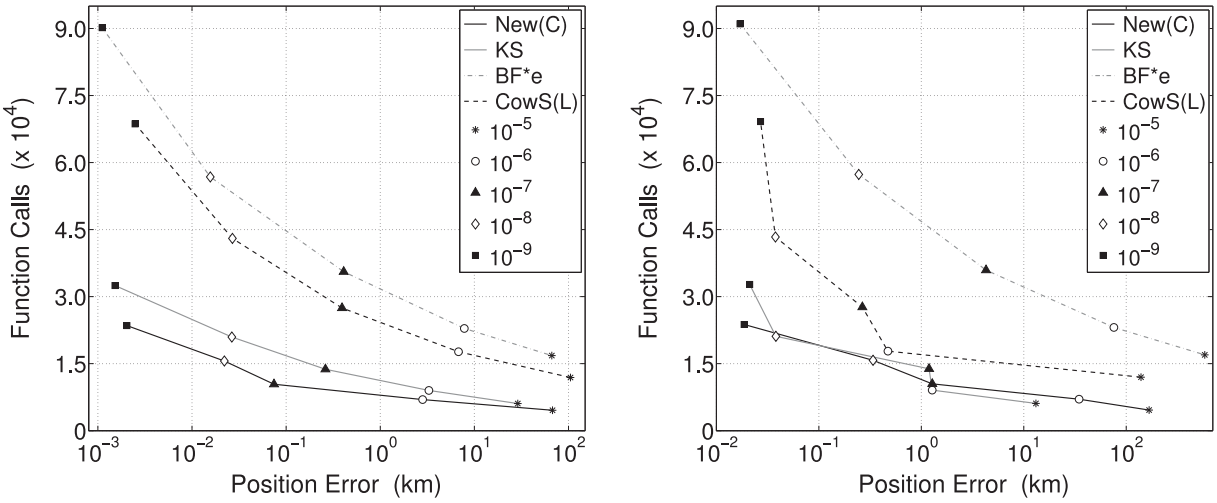

Figure 7. Function calls versus position error after about 49.5 (left-hand) and 50 (right-hand) revolutions (the exact intervals of time are given in Table 3); example 3: artificial satellite of the Earth perturbed by J_2, Moon, solar radiation pressure, atmospheric drag. The numerical integrator is the 5th-order explicit Runge–Kutta method (DOPRI54). The relative tolerance is changed from 10^{-5} to 10^{-9} and the absolute tolerance is set to 10^{-13}. Since the formulations that use orbital elements exhibit similar performance, only the curves of New(C) are displayed.

Table 4. Example 3; total number of function calls for a very accurate propagation until the epoch $t_{\mathrm{ref},1}$ (Table 3). The relative and absolute tolerance of the numerical integrator DOPRI54 are both set to 10^{-13}. In the brackets, the computational cost is normalized with respect to the function calls of New(L). We report only the methods for which the distance between the final and reference positions is between 0.7 and 1.3 m.

Formulations	Function calls		Formulations	Function calls	
New(L)	63715	(1)	Dromo(PC)a	189475	(2.97)
New	64375	(1.01)	KS	191317	(3.00)
Dromo(PL)e	76627	(1.20)	Stiefel(C)	228379	(3.58)
Stiefel*(L)	115663	(1.82)	BF*(L)e	357547	(5.61)
New(C)	130423	(2.05)	BF*e	358909	(5.63)
Sti&Sche	131851	(2.07)	BF*(C)e	387403	(6.08)
Stiefel*(C)	180997	(2.84)	CowS(L)	443365	(6.96)
Dromo(PC)e	186277	(2.92)			

Table 5. Position error at the epoch $t_{\mathrm{ref},1}$ (Table 3) for 160, 320, 640 steps per nominal period; example 3. The numerical integrators are the 10th-order multistep methods ABM, SC-ABM, and the symbols !, !! indicate the use of the ABM, SC-ABM, respectively. We provide also the time (average value over 20 runs) spent to numerically integrate the system of differential equations from the initial to the final state vector. The total number of steps is given by (160, 320, 640) times 49.5.

Formulations	Position error (km)			Time (s)		
	160	320	640	160	320	640
New	0.380	0.055	0.033	1.72	3.41	6.80
Sti&Sche	0.342	0.055	0.033	1.75	3.48	6.93
Stiefel*(C)	0.421	0.037	0.026	1.77	3.50	7.02
KS!	0.215	0.039	0.026	1.70	3.38	6.74
CowS(L)!	0.235	0.039	0.026	1.57	3.12	6.24
Dromo(PC)e	11.225	0.018	0.001	1.75	3.48	6.92
BF*(L)a!!	21.946	0.013	0.001	2.35	4.64	9.26

Table 6. Same as Table 5, but for the time interval $t_{\mathrm{ref},2}$ (Table 3). The total number of steps is given by (160, 320, 640) times 50.

Formulations	Position error (km)		
	160	320	640
New	7.15	0.88	0.28
Sti&Sche	6.29	0.88	0.28
Stiefel*(C)	5.96	0.81	0.42
KS!	4.90	0.85	0.42
CowS(L)!	5.21	0.85	0.42
Dromo(PC)e	267.02	0.75	0.01
BF*a!!	506.11	1.44	0.01

much bigger for Dromo(PL)e and BF*a already after a few nominal periods, and the gap enlarges because of the faster error growth. Among the other formulations, which are comparable in terms of accumulated error, the best behaviour is shown by New(C) and Sti&Sche, especially in the first one thousand nominal revolutions.

7.5 Additional comments

Some additional comments about the numerical tests are listed below. (1) We discovered that the use of the total energy instead of the generalized angular momentum in the B–F linearization (Appendix C) is much more advantageous when the formulation is combined to the DOPRI54 integrator. (2) The methods named Stiefel*(C) and Stiefel*(L) (Appendix C), which are proposed here for the first time, are always better than Stiefel(C). (3) The constant and linear time elements developed for the new method (Section 4) do not bring a significant benefit with the ABM integrator. (4) CowS(L) is always more efficient than CowS, that is the linear time element is effective at stabilizing the differential equation of the physical time. (5) For the methods CowS, BF, and BF* we also tried to obtain the physical time by integration of a second-order differential equation. It turns out that this option is never convenient.

8 CONCLUSIONS

New orbital elements are developed for computing special perturbations in the two-body problem. The projective decomposition of the motion into the radial displacement and into the rotation of the radial unit vector, which is borrowed from the Burdet–Ferrándiz linearization, is carried out with a classical Sundman transformation of the physical time. It is known that the orbital radius is a regular variable with respect to the adopted fictitious time. Taking advantage of this fact the first two elements are derived after applying the VOP method to the radial equation of motion. The geometrical meaning of the new quantities invites to define an intermediate frame, which, as far as we know, has never been discovered before. This frame remains fixed when the perturbations are absent and, in general, it differs from the local vertical local horizontal frame by one rotation around the direction of the angular momentum vector. Four Euler parameters describing the attitude of the intermediate frame are chosen as elements of the new method. They bring information on the orbital plane and on the departure direction for the orbital longitude of the propagated object. We show that also these four elements can be obtained from a set of linear differential equations (in the two-body problem) via the VOP method. The six elements and the total energy, which is assumed to be negative, allow us to completely characterize the motion in the fictitious time. A linear and a constant time element is supplied to recover the physical

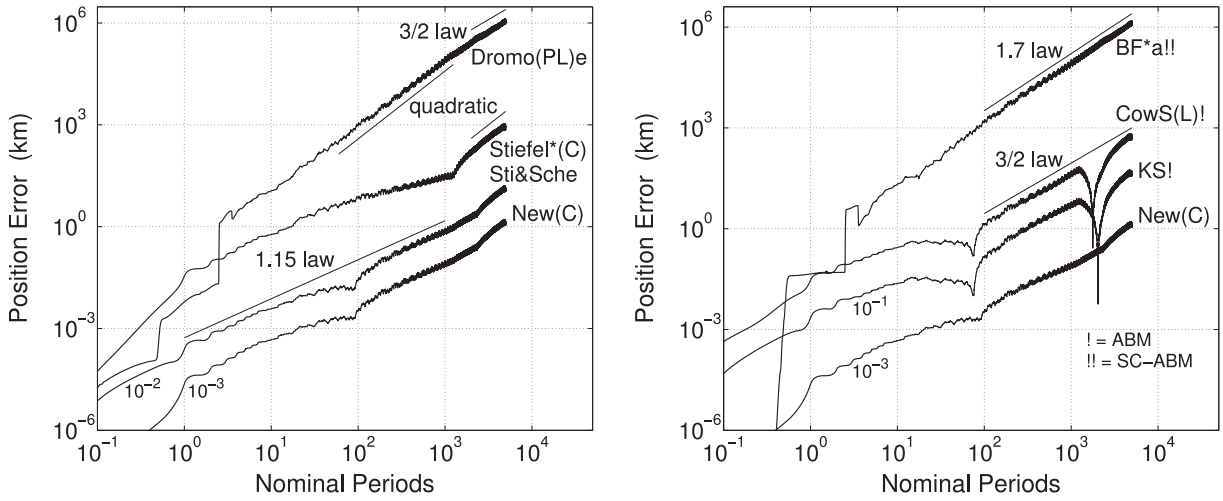

Figure 8. Position error accumulated during 5000 nominal periods; example 3: artificial satellite of the Earth perturbed by J_2, Moon, solar radiation pressure, atmospheric drag. The new method is compared with the formulations based on elements (left-hand) and on coordinates (right-hand). The numerical integrators are the 10th-order multistep methods ABM, SC-ABM, and the number of steps per nominal period is 160. To avoid superpositions, the curves are shifted along the vertical axis by a suitable power of 10 when necessary.

time. The final set of eight orbital elements is non-singular for zero eccentricity, inclination, and non-zero angular momentum.

The performance of the new method was assessed by considering perturbed scenarios around the Sun and the Earth. Two algorithms representative of a variable and a fixed step-size integrator were selected. The proposed elements are much more efficient than the schemes exploiting a time transformation in which the orbital radius is squared. The only exception is for a short-term propagation with a fixed step of a geocentric motion perturbed by the Earth's oblateness, the Moon's attraction, the solar radiation pressure, and the atmospheric drag. In this case, the highest accuracy with the smallest computational cost is achieved by Dromo(PC) with the total energy as one of the state variables (Baù & Bombardelli 2014). It is impressive that the new method can become substantially more efficient than the Kustaanheimo-Stiefel regularization and the related sets of regular elements included in the comparison. Moreover, these formulations are never better than the new scheme in all the numerical tests. The introduction of a time element is effective only with a variable step-size integrator, and, in particular, we noted that by employing a linear time element the computational cost at high accuracies is lower with respect to the other methods. Finally, it deserves to be said that we present new improved versions of the original B–F method and of Stiefel's set of spatial elements completed by a time element (Arakida & Fukushima 2001).

REFERENCES

Arakida H., Fukushima T., 2001, AJ, 121, 1764
Barrio R., Serrano S., 2008, Math. Comput. Modelling, 48, 594
Baù G., Bombardelli C., 2014, AJ, 148, 1
Baù G., Bombardelli C., Peláez J., 2013, Celest. Mech. Dyn. Astron., 116, 53
Baumgarte J., 1972, Celest. Mech., 5, 490
Bond V. R., 1974, Celest. Mech., 10, 303
Bond V. R., Allman M. C., 1996, Modern Astrodynamics: Fundamentals and Perturbation Methods. Princeton Univ. Press, Princeton, NJ
Broucke R. A., Cefola P., 1972, Celest. Mech., 5, 303
Broucke R., Lass H., Ananda M., 1971, A&A, 13, 390
Brown E. W., 1896, An Introductory Treatise on the Lunar Theory. Cambridge Univ. Press, Cambridge
Burdet C. A., 1967, Z. Angew. Math. Phys., 18, 434
Burdet C. A., 1968, Z. Angew. Math. Phys., 19, 345
Burdet C. A., 1969, J. Reine Angew. Math., 238, 71
Cayley A., 1843, Camb. Math. Journal, 3, 224
Chelnokov Y. N., 1992, Kosm. Issled., 30, 759
Chelnokov Y. N., 1993, Kosm. Issled., 31, 3
Cohen C. J., Hubbard E. C., 1962, AJ, 67, 10
Dallas S. S., Rinderle E. A., 1974, J. Astronaut. Sci., 21, 129
Deprit A., 1975, J. Res. Nat. Bur. Stand. B, 79B, 1
Deprit A., 1976, Celest. Mech., 13, 253
Dormand J. R., Prince P. J., 1980, J. Comput. Appl. Math., 6, 19
Ferrándiz J. M., 1988, Celest. Mech., 41, 343
Ferrándiz J. M., Sansaturio M. E., Vigo J., 1991, in Roy A. E., ed., NATO ASI Series, Vol. 272, Predictability, Stability, and Chaos in N-Body Dynamical Systems. Plenum Press, New York, NY, p. 387
Flury W., Janin G., 1975, Astrophys. Space Sci., 36, 495
Fukushima T., 2004a, AJ, 128, 3108
Fukushima T., 2004b, AJ, 128, 3114
Fukushima T., 2007a, AJ, 133, 1
Fukushima T., 2007b, AJ, 133, 2815
Fukushima T., 2008, AJ, 135, 72
Garofalo A. M., 1960, AJ, 65, 117
Gurfil P., 2005, J. Guid. Control Dyn., 28, 1079
Hairer E., Nørsett S. P., Wanner G., 2009, Solving Ordinary Differential Equations I: Nonstiff Problems. Springer-Verlag, Berlin
Hansen P. A., 1857, Abh. Kön. Sächs. Ges. Wiss. Leipzig, 5, 41
Henrici P., 1962, Discrete Variable Methods in Ordinary Differential Equations. Wiley, New York
Herget P., 1962, AJ, 67, 16
Herrick S., 1948, PASP, 60, 321
Herrick S., 1953, AJ, 58, 156
Hestenes D., 1983, Celest. Mech., 30, 151
Hintz G. R., 2008, J. Guid. Control Dyn., 31, 785
Janin G., 1974, Celest. Mech., 10, 451
Kustaanheimo P., Stiefel E. L., 1965, J. Reine Angew. Math., 218, 204
Marsden B. G., 1980, Celest. Mech., 22, 63
Milani A., Gronchi G. F., 2010, Theory of Orbit Determination. Cambridge Univ. Press, Cambridge
Milanković M., 1939, Bull. Acad. Sci. Math. Nat., 6, 1
Montenbruck O., Gill E., 2000, Satellite Orbits – Models, Methods and Applications, 1st edn. Springer, the Netherlands
Musen P., 1954, AJ, 59, 262
Musen P., 1958, AJ, 63, 426

Musen P., 1960, J. Geophys. Res., 65, 1391
Musen P., 1961a, J. Astronaut. Sci., 8, 48
Musen P., 1961b, J. Geophys. Res., 66, 2797
Musen P., 1964, NASA Technical Report TN D-2301, On the Application of Pfaff's Method in the Theory of Variation of Astronomical Constants. NASA, Washington, DC
Palacios M., Calvo C., 1996, J. Astronaut. Sci., 44, 63
Peláez J., Hedo J. M., de Andrés P. R., 2007, Celest. Mech. Dyn. Astron., 97, 131
Pines S., 1961, AJ, 66, 5
Rodrigues O., 1840, J. Math. Pures Appl., 5, 380
Rosengren A. J., Scheeres D. J., 2014, Celest. Mech. Dyn. Astron., 118, 197
Sharaf M. A., Awad M. E., Najmuldeen S. A. A., 1992, Earth Moon Planets, 56, 141
Sperling H., 1961, Am. Rocket Soc. J., 31, 660
Stiefel E. L., Scheifele G., 1971, Linear and Regular Celestial Mechanics. Springer-Verlag, Berlin
Stiefel E., Rössler M., Waldvogel J., Burdet C. A., 1967, NASA Technical report CR-769, Methods of Regularization for Computing Orbits in Celestial Mechanics. NASA, Washington, DC
Strömgren B., 1929, Publ. og mindre Medd. fra Köbenhavns Obs., 65, 3
Velez C. E., Cefola P. J., Long A. C., Nimitz K. S., 1974, in Bettis D. G., ed., Lecture Notes in Mathematics, Vol. 362, Proceedings of the Conference on the Numerical Solution of Ordinary Differential Equations. Springer-Verlag, Berlin, p. 183
Vitins M., 1978, Celest. Mech., 17, 173
Whittaker E. T., 1917, A Treatise on the Analytical Dynamics of particles and rigid bodies, 2nd edn. Cambridge Univ. Press, Cambridge
Wilson E. B., 1901, Vector Analysis. Yale Univ. Press, New Haven

APPENDIX A

A1 Expression of v (equation 5.15)

We start from the well-known formula

$$\tan\left(\frac{\theta-G}{2}\right)=\frac{\sin\theta-\sin G}{\cos\theta+\cos G}. \tag{A1}$$

By use of equations (5.4), (5.5), (3.10), and (3.14) we end up after some simplifications with

$$\theta-G=2\arctan\left(\frac{\frac{\mathrm{d}r}{\mathrm{d}\varphi}}{c\sqrt{\lambda_3}+r}\right). \tag{A2}$$

Equation (5.3) is solved for the generalized angular momentum c, and by considering the relation $g^2=\lambda_1^2+\lambda_2^2$, which follows from (5.6) and (5.7), we have

$$c=\sqrt{\lambda_3\left(1-\lambda_1^2-\lambda_2^2\right)}. \tag{A3}$$

Finally, by means of equations (3.17), (3.18), and (A3), and replacing $\theta-G$ with $\nu-\varphi$ (see equation 5.11), we can write (A2) into the form shown in equation (5.15).

A2 Expression of $\frac{\mathrm{d}v}{\mathrm{d}\varphi}$ (equation 5.20)

Consider the identity

$$\left(\frac{c^2}{r}-1\right)\boldsymbol{i}-c\,\frac{\mathrm{d}r}{\mathrm{d}t}\,\boldsymbol{j}=\lambda_1\boldsymbol{x}+\lambda_2\boldsymbol{y}, \tag{A4}$$

where both sides represent the generalized eccentricity vector $\boldsymbol{g}$: the left one is derived from equations (5.1) and (5.2), and the right one is the expression in (5.8). After rearranging the terms, differentiation of equation (A4) referred to the intermediate frame $\{\mathrm{F};\boldsymbol{x},\boldsymbol{y},\boldsymbol{k}\}$ gives

$$\frac{\mathrm{d}v}{\mathrm{d}\varphi}\,g\,\boldsymbol{e}_b=\frac{\mathrm{d}\lambda_1}{\mathrm{d}\varphi}\,\boldsymbol{x}+\frac{\mathrm{d}\lambda_2}{\mathrm{d}\varphi}\,\boldsymbol{y}+\frac{\mathrm{d}}{\mathrm{d}\varphi}\left(1-\frac{c^2}{r}\right)\boldsymbol{i}+\frac{\mathrm{d}}{\mathrm{d}\varphi}\left(c\,\frac{\mathrm{d}r}{\mathrm{d}t}\right)\boldsymbol{j}, \tag{A5}$$

with $g=|\boldsymbol{g}|$ and

$$g\,\boldsymbol{e}_b=\boldsymbol{k}\times\boldsymbol{g}=c\,\frac{\mathrm{d}r}{\mathrm{d}t}\,\boldsymbol{i}+\left(\frac{c^2}{r}-1\right)\boldsymbol{j}. \tag{A6}$$

Note that the relative angular velocity $\boldsymbol{\omega}_{\mathcal{IO}}$ (equation 5.12) is employed in the Poisson's formulae for $\boldsymbol{i}$ and $\boldsymbol{j}$.

The radial acceleration (3.7) is put in the form

$$\frac{\mathrm{d}^2r}{\mathrm{d}t^2}=\frac{c^2}{r^3}-\frac{1}{r^2}+R-\frac{2\mathcal{U}}{r}, \tag{A7}$$

where we made appear the generalized angular momentum c (see 5.2). Equations (3.8), (A6), and (A7) are used to write

$$\frac{\mathrm{d}}{\mathrm{d}\varphi}\left(1-\frac{c^2}{r}\right)\boldsymbol{i}+\frac{\mathrm{d}}{\mathrm{d}\varphi}\left(c\,\frac{\mathrm{d}r}{\mathrm{d}t}\right)\boldsymbol{j}=\frac{\mathrm{d}c}{\mathrm{d}\varphi}\left(\frac{\mathrm{d}r}{\mathrm{d}t}\,\boldsymbol{j}-\frac{2\,c}{r}\,\boldsymbol{i}\right)+\frac{c}{\sqrt{-2\,\varepsilon}}\left[\frac{g}{r}\,\boldsymbol{e}_b+(R\,r-2\mathcal{U})\,\boldsymbol{j}\right]. \tag{A8}$$

Since the unit vector $\boldsymbol{e}_b$ satisfies

$$\boldsymbol{e}_b\cdot\boldsymbol{x}=-\sin(\varphi-G),\quad \boldsymbol{e}_b\cdot\boldsymbol{y}=\cos(\varphi-G), \tag{A9}$$

$$\boldsymbol{e}_b\cdot\boldsymbol{i}=\sin\theta,\quad \boldsymbol{e}_b\cdot\boldsymbol{j}=\cos\theta, \tag{A10}$$

scalar multiplication by $\boldsymbol{e}_b$ of equation (A5), modified according to (A8), produces

$$\frac{\mathrm{d}v}{\mathrm{d}\varphi}\,g=\frac{\mathrm{d}\lambda_2}{\mathrm{d}\varphi}\cos\beta-\frac{\mathrm{d}\lambda_1}{\mathrm{d}\varphi}\sin\beta+\frac{\mathrm{d}c}{\mathrm{d}\varphi}\left(\frac{\mathrm{d}r}{\mathrm{d}t}\cos\theta-\frac{2c}{r}\sin\theta\right)+\frac{c}{\sqrt{-2\,\varepsilon}}\left[\frac{g}{r}+(R\,r-2\mathcal{U})\cos\theta\right], \tag{A11}$$

where $\beta=\varphi-G$. With the help of equations (3.23), (3.24), (5.6), and (5.7) we get

$$\frac{\mathrm{d}\lambda_2}{\mathrm{d}\varphi}\cos\beta-\frac{\mathrm{d}\lambda_1}{\mathrm{d}\varphi}\sin\beta=(2\mathcal{U}-R\,r)\,\frac{r}{g}\,(1-\varrho)+\frac{\mathrm{d}\lambda_3}{\mathrm{d}\varphi}\,\frac{\zeta}{2\,\lambda_3\,g}\,(1+\varrho), \tag{A12}$$

and differentiation of equation (A3) yields

$$\frac{\mathrm{d}c}{\mathrm{d}\varphi}=\frac{\sqrt{\lambda_3}\varrho}{m}\left[(2\mathcal{U}-R\,\lambda_3\varrho)\,\lambda_3\zeta+\frac{\mathrm{d}\lambda_3}{\mathrm{d}\varphi}\,\frac{\varrho}{2\,\lambda_3}\right]. \tag{A13}$$

Moreover, by using equations (5.4) and then (3.10), (3.14), (3.17), (3.18), (A3), we find

$$\frac{\mathrm{d}r}{\mathrm{d}t}\cos\theta-\frac{2\,c}{r}\sin\theta=-\left(\frac{m^2}{\varrho}+1\right)\frac{\zeta}{g\,\sqrt{\lambda_3\varrho}}, \tag{A14}$$

and

$$\frac{c}{\sqrt{-2\,\varepsilon}}\left[\frac{g}{r}+(R\,r-2\mathcal{U})\cos\theta\right]=\frac{m}{\varrho}\left[g+\frac{\lambda_3}{g}\,(R\,r-2\mathcal{U})\,(m^2-\varrho)\right], \tag{A15}$$

where m is given in (6.11).

Finally, the expressions derived in equations (A12)–(A15) are plugged into (A11), we divide by g and apply the substitutions $\zeta^2=\varrho(2-\varrho)-m^2$, $g^2=1-m^2$ to find equation (5.20).

APPENDIX B: COMPUTATION OF λ_4, λ_5, λ_6, λ_7

When $\lambda_7 = 0$, equations (6.37) become singular. In this case, the other Euler parameters are computed as follows:

$$\lambda_4 = \frac{k_1}{2\,\lambda_6}, \quad \lambda_5 = \frac{k_2}{2\,\lambda_6}, \quad \lambda_6 = \sqrt{\frac{1+k_3}{2}}. \tag{B1}$$

If also $\lambda_6 = 0$, then we use

$$\lambda_4 = \sqrt{\frac{1-y_2}{2}}, \quad \lambda_5 = \frac{y_1}{2\,\lambda_4}. \tag{B2}$$

Finally, if even $\lambda_4 = 0$ then we set $\lambda_5 = 1$.

APPENDIX C

C1 Modified Stiefel's elements completed by a time element

The original method of Stiefel (Stiefel et al. 1967, p. 18) consists of ten state variables: the physical time t, the variation W of the instantaneous Keplerian energy per unit mass (ε_K) from its initial value ($\varepsilon_{K,0}$), and eight elements related to the vector $\boldsymbol{u}$ of the four K-S parameters. Arakida & Fukushima (2001) in the appendix of their paper proposed to complete Stiefel's elements with a time element instead of the physical time. Here, we generalize these ten elements with the aim of improving their performance in orbit computation. Moreover, we also develop an alternative time element.

We start from equation A1 in Arakida & Fukushima (2001):

$$\frac{\mathrm{d}^2\boldsymbol{u}}{\mathrm{d}s^2} + w_0^2\,\boldsymbol{u} = \boldsymbol{F}, \tag{C1}$$

where the independent variable s is introduced by the time transformation $\mathrm{d}t = r\,\mathrm{d}s$, with r the orbital radius. The interesting fact in equation (C1) is that the frequency w_0 of the perturbed harmonic oscillator is always a constant, while in the most known form of the differential equation for $\boldsymbol{u}$ (Stiefel & Scheifele 1971, p. 30, equation 51) the frequency can be changed by the perturbations. More specifically, we have

$$w_0^2 = -\frac{\varepsilon_{K,0}}{2}, \quad \boldsymbol{F} = \frac{1}{4}\,(r\,\boldsymbol{q} + 2\,W\boldsymbol{u}), \tag{C2}$$

where

$$\boldsymbol{q} = -\frac{\partial\,\mathcal{U}}{\partial\,\boldsymbol{u}} + 2\,\mathbf{L}^T\boldsymbol{f}, \quad W = \varepsilon_K - \varepsilon_{K,0}, \tag{C3}$$

being $\mathbf{L} \in \mathbb{R}^{4\times4}$ the K–S matrix (Stiefel & Scheifele 1971, p. 24, equation 27), $\mathcal{U}$ the disturbing potential energy per unit mass, and $\boldsymbol{f}$ a vector with the first three components given by $\boldsymbol{P}$ (see equation 3.2) and a vanishing fourth component.

We suggest to employ the initial value of the total energy per unit mass (ε_0) in the definition of w_0 (equation C2). By applying this change, equation (C1) holds with

$$w_0^2 = -\frac{\varepsilon_0}{2}, \quad \boldsymbol{F} = \frac{1}{4}\,[\,r\,\boldsymbol{q} + 2\,(W - \mathcal{U})\,\boldsymbol{u}\,], \tag{C4}$$

where $\boldsymbol{q}$ is given in (C3) and

$$W = \varepsilon - \varepsilon_0, \tag{C5}$$

being $\varepsilon = \varepsilon_K + \mathcal{U}$. The quantity W in equation (C5) is one of the elements of the improved formulation and its derivative with respect to s reads (Stiefel & Scheifele 1971, p. 31, see the equation for h in 53)

$$\frac{\mathrm{d}W}{\mathrm{d}s} = \frac{\partial\,\mathcal{U}}{\partial\,t}r + 2\frac{\mathrm{d}\boldsymbol{u}}{\mathrm{d}s}\cdot\mathbf{L}^T\boldsymbol{f}. \tag{C6}$$

The other elements are the time element (t_0) and the four-dimensional vectors ($\boldsymbol{\alpha}$, $\boldsymbol{\beta}$) related to the K–S parameters $\boldsymbol{u}$. The definitions of $\boldsymbol{\alpha}$, $\boldsymbol{\beta}$, t_0, and their differential equations are the same as in equations A3, A5, and A6 of Arakida & Fukushima (2001), wherein w_0 and $\boldsymbol{F}$ take the expressions in (C4).

Finally, we propose an other time element, which can be used in place of t_0. Kepler's equation written in terms of Stiefel's elements becomes (equation A4):

$$t = t_0 + \frac{\boldsymbol{\alpha}^2 + \boldsymbol{\beta}^2}{2}s + \frac{\boldsymbol{\alpha}^2 - \boldsymbol{\beta}^2}{4w_0}\sin(2w_0 s) - \frac{\boldsymbol{\alpha}\cdot\boldsymbol{\beta}}{2w_0}\cos(2w_0 s). \tag{C7}$$

The new time element is defined as

$$t_1 = t_0 + \frac{\boldsymbol{\alpha}^2 + \boldsymbol{\beta}^2}{2}s, \tag{C8}$$

where t_0 is a constant along a Keplerian motion, while t_1 varies linearly with s. From equations (C8) and A6 we find

$$\frac{\mathrm{d}t_1}{\mathrm{d}s} = \frac{\boldsymbol{\alpha}^2 + \boldsymbol{\beta}^2}{2} + \frac{\boldsymbol{F}\cdot\boldsymbol{u}}{2w_0^2}. \tag{C9}$$

C2 Modified B–F regularization

Burdet (1969) introduced a transformation from the position vector $\boldsymbol{r}$ to the reciprocal radius $\rho = \frac{1}{r}$ and the radial unit vector $\boldsymbol{i} = \frac{\boldsymbol{r}}{r}$. Changing the independent variable through the time transformation

$$\frac{\mathrm{d}t}{\mathrm{d}\phi} = \frac{1}{\xi\,\rho^2}, \tag{C10}$$

where ξ is a constant in the two-body problem, converts the differential equations of ρ and $\boldsymbol{i}$ into four perturbed harmonic oscillators with common frequency w. The position and velocity can be fully described by ρ, $\boldsymbol{i}$, their derivatives with respect to ϕ, and the semi-latus rectum p. If $\xi = 1$, like in Burdet (1969), then w is the angular momentum per unit mass h, while if $\xi = h$, we have a unitary frequency. The latter choice for ξ was made by Burdet in a later unpublished paper (see Flury & Janin 1975), and the resulting differential equations for t, ρ, $\boldsymbol{i}$, and p can be found in Vitins (1978, section 2). Burdet's linearization was developed in the Hamiltonian formalism by Ferrándiz (1988), and it is usually referred to as B–F regularization.

We propose a modified version of the B–F method which, as we have only recently discovered, was also investigated by Vitins (1978, section 4). Reference units for length and time are employed for which the constant $k^2(m+M)$ becomes equal to 1 (see equation 3.1). Let $\xi = c$, where c is the generalized angular momentum (see 5.2), so that equation (C10) represents the same time transformation as in Baù et al. (2013, equation 3). The differential equations of ρ, $\boldsymbol{i}$, c are

$$\frac{\mathrm{d}\rho}{\mathrm{d}\phi} = \sigma, \qquad \frac{\mathrm{d}\boldsymbol{i}}{\mathrm{d}\phi} = \boldsymbol{u}, \tag{C11}$$

$$\frac{\mathrm{d}\sigma}{\mathrm{d}\phi} = -\rho + \frac{1}{c^2} + \frac{1}{c}\left(f\,s - \frac{\mathrm{d}c}{\mathrm{d}\phi}\sigma\right), \tag{C12}$$

$$\frac{\mathrm{d}\boldsymbol{u}}{\mathrm{d}\phi} = -\boldsymbol{i} + s^2\,(\boldsymbol{F}\,r + f\,\boldsymbol{i}) - \frac{1}{c}\frac{\mathrm{d}c}{\mathrm{d}\phi}\boldsymbol{u}, \tag{C13}$$

$$\frac{\mathrm{d}c}{\mathrm{d}\phi} = s\,r^2\left[\boldsymbol{P}\cdot\boldsymbol{u} + \frac{\partial\,\mathcal{U}}{\partial\,t}s - \left(2\mathcal{U} + r\frac{\partial\,\mathcal{U}}{\partial\,\boldsymbol{r}}\cdot\boldsymbol{i}\right)\sigma\right], \tag{C14}$$

where the quantities $\boldsymbol{F}$, $\boldsymbol{P}$, $\mathcal{U}$ are defined as in equations (3.1) and (3.2), and

$$s = \frac{1}{c\,\rho}, \quad f = 2\mathcal{U} - r\,\boldsymbol{F}\cdot\boldsymbol{i}. \tag{C15}$$

Equations (C12) and (C14) are reported, in a slightly different form, also in Baù et al. (2013) and in Vitins (1978). Note that the velocity vector is obtained by the formula $\boldsymbol{v} = c\,(\rho\,\boldsymbol{u} - \sigma\,\boldsymbol{i})$ wherein the potential $\mathcal{U}$ does not explicitly appear. The total energy ε (equation 3.9) can be selected as an alternative state variable to c. In this case we have to add to (C10)–(C13), (C15) the two equations

$$\frac{\mathrm{d}\varepsilon}{\mathrm{d}\phi} = r\left[\boldsymbol{P}\cdot(\boldsymbol{u} - \sigma\,r\,\boldsymbol{i}) + \frac{\partial\,\mathcal{U}}{\partial\,t}s\right], \quad c = \sqrt{2\,\frac{\varepsilon+\rho}{\rho^2+\sigma^2}}. \tag{C16}$$

Following Baù & Bombardelli (2014), we define a linear and a constant time element as

$$t_1 = t + \frac{c\,r\,\sigma}{2\,\varepsilon} + \frac{k_0}{\varepsilon\sqrt{-2\,\varepsilon}}, \qquad k_0 = \arctan\left(\frac{c\,\sigma}{c\,\rho + \sqrt{-2\,\varepsilon}}\right), \tag{C17}$$

$$t_0 = t_1 - \frac{\phi}{(-2\,\varepsilon)^{3/2}}, \tag{C18}$$

which are governed by the differential equations

$$\frac{\mathrm{d}t_1}{\mathrm{d}\phi} = \frac{1}{(-2\,\varepsilon)^{3/2}}\left[1 + \frac{\mathrm{d}\varepsilon}{\mathrm{d}\phi}\left(\frac{3}{\varepsilon}k_0 + k_1\right) - f\,k_2\right], \tag{C19}$$

$$\frac{\mathrm{d}t_0}{\mathrm{d}\phi} = \frac{1}{(-2\,\varepsilon)^{3/2}}\left\{\frac{\mathrm{d}\varepsilon}{\mathrm{d}\phi}\left[\frac{3}{\varepsilon}\left(k_0 + \frac{\phi}{2}\right) + k_1\right] - f\,k_2\right\}, \tag{C20}$$

where

$$k_1 = -\frac{\sigma\,s}{\sqrt{-2\,\varepsilon}}\left(\frac{r+c^2}{1+c\sqrt{-2\,\varepsilon}} + 2\,c^2 - r\right),$$

$$k_2 = s^2\left(\frac{1+2\,\varepsilon\,r}{1+c\sqrt{-2\,\varepsilon}} + 1 + c\sqrt{-2\,\varepsilon}\right). \tag{C21}$$

Either equations (C17) and (C19), which were derived also by Vitins (1978), or equations (C18) and (C20), which are proposed here for the first time, can substitute equation (C10).

This paper has been typeset from a TEX/LATEX file prepared by the author.